Renal tubule Cpt1a overexpression mitigates kidney fibrosis by restoring mitochondrial homeostasis

Verónica Miguel[1], Jessica Tituaña[1], J.Ignacio Herrero[1], Laura Herrero[2,3], Dolors Serra[2,3], Paula Cuevas[4], Coral Barbas[4], Diego Rodríguez Puyol[5], Laura Márquez-Exposito[6], Marta Ruiz-Ortega[6], Carolina Castillo[7], Xin Sheng[8], Katalin Susztak[8], Miguel Ruiz-Canela[9,10], Jordi Salas-Salvadó[10,11], Frank B. Hu[12,13], Miguel A. Martínez Gonzalez[9,10,12], Sagrario Ortega[14], Ricardo Ramos[15], Santiago Lamas[1]*

1. Programme of Physiological and Pathological Processes, Centro de Biología Molecular "Severo Ochoa" (CSIC-UAM), 28049 Madrid, Spain.
2. Department of Biochemistry and Physiology, School of Pharmacy and Food Sciences, Institut de Biomedicina de la Universitat de Barcelona (IBUB), Universitat de Barcelona, E-08028, Barcelona, Spain.
3. Centro de Investigación Biomédica en Red de Fisiopatología de la Obesidad y la Nutrición (CIBEROBN), Instituto de Salud Carlos III, E-28029 Madrid, Spain
4. Centre for Metabolomics and Bioanalysis (CEMBIO), Chemistry and Biochemistry Department, Pharmacy Faculty, Universidad San Pablo-CEU, Boadilla del Monte, 28668 Madrid, Spain.
5. Department of Medicine and Medical Specialties, Research Foundation of the University Hospital "Príncipe de Asturias," IRYCIS, Alcalá University, Alcalá de Henares, Madrid, Spain.
6. Cellular and Molecular Biology in Renal and Vascular Pathology Laboratory. Fundación Instituto de Investigación Sanitaria-Fundación Jiménez Díaz-Universidad Autónoma Madrid, Madrid, Spain.
7. University Hospital "Príncipe de Asturias, Alcalá de Henares, Madrid, Spain.

8. Division of Nephrology, Department of Medicine, Department of Genetics, Perelman School of Medicine, University of Pennsylvania, Philadelphia, PA, USA.
9. University of Navarra, Department of Preventive Medicine and Public Health, IdiSNA (Health Research Institute of Navarra), Pamplona, Spain
10. CIBER de Fisiopatología de la Obesidad y Nutrición (CIBEROBN), Instituto de Salud Carlos III, Madrid, Spain
11. Human Nutrition Unit, Faculty of Medicine and Health Sciences, Pere Virgili Health Research Institute, Rovira i Virgili University, Reus, Spain
12. Department of Nutrition, Harvard T.H. Chan School of Public Health, Boston, MA, USA
13. Channing Division of Network Medicine, Department of Medicine, Brigham and Women's Hospital and Harvard Medical School, Boston, Massachusetts, USA
14. Transgenics Unit, Spanish National Cancer Research Centre (CNIO), Madrid 28029, Spain.
15. Genomic Facility, Parque Científico de Madrid, Madrid, Spain.

*Correspondence: Santiago Lamas (slamas@cbm.csic.es).

Abstract

Chronic kidney disease (CKD) remains a major epidemiological, clinical and biomedical challenge. During CKD, renal tubular epithelial cells (TECs) suffer a persistent inflammatory and profibrotic response. Defective fatty acid oxidation (FAO), the main source of energy for TECs, contributes to kidney fibrosis. To determine if FAO gain-of-function (FAO-GOF) could protect from fibrosis, we generated a conditional transgenic mouse model with overexpression of the fatty acid shuttling enzyme carnitine palmitoyl-transferase 1 A (CPT1A) in TECs. *Cpt1a* knock-in mice subjected to three different models of renal fibrosis exhibited decreased expression of fibrotic markers, a blunted pro-inflammatory response and reduced epithelial cell damage. Mitochondrial number, oxygen consumption and ATP levels were restored after FAO-GOF. Studies in patients evidenced decreased CPT1 levels and increased accumulation of short and middle chain acylcarnitines, reflecting impaired FAO in human CKD. We propose that strategies based on FAO-GOF may constitute powerful alternatives to combat fibrosis inherent to CKD.

Introduction

Organ fibrosis constitutes a significantly prevalent pathological entity associated to high morbidity and mortality and a major biomedical challenge. While it may affect any tissue of the human body, its presence in the kidney generally indicates unrelenting progression to chronic renal failure, a condition associated to reduced expectancy and quality of life. Hence, fibrosis is a convergent pathway for prevalent pathologies underlying chronic kidney disease (CKD) such as diabetes, hypertension or nephrosclerosis [1]. Beyond proper blood pressure and glycemic controls, therapeutic options to revert or deter the progression of fibrosis are very limited. In the last few years, the understanding of major metabolic disturbances coexisting with kidney fibrosis have shed new light on the pathogenesis of fibrosis progression [2]. Among these, a drastic reduction in fatty acid oxidation (FAO) appears to be critical for the global energy failure occurring in the tubulo-interstitial compartment, contributing to immune cell infiltration and kidney fibrosis [3,4]. Here we tested whether specific metabolic gain-of-function in FAO in renal tubules was necessary and sufficient to counteract cellular and molecular changes associated to kidney fibrosis. Carnitine palmitoyl transferase 1A (CPT1A) is a rate-limiting and targetable enzyme in this pathway. We found that conditional overexpression of CPT1A resulted in significant mitigation of fibrosis and improvement of renal function in three different experimental models. This was related to enhanced mitochondrial mass, repaired architecture and bioenergetics recovery. The overexpression of CPT1A was also associated with a reduced inflammatory pattern and abrogation of TGF-beta-induced epithelial cell damage. Moreover, studies in patients showed that a reduction in the levels of CPT1A correlated with the degree of fibrosis. In addition, in a large cohort of diabetic patients with CKD a specific profile of increased plasma acylcarnitines was found, reinforcing the critical metabolic derangement of FAO associated to CKD.

Results

Overexpression of tubular CPT1A results in phenotypic protection against kidney fibrosis.

To test the *in vivo* relevance of CPT1A and FAO for renal fibrosis, a mouse model with conditional, inducible expression of *Cpt1a* was engineered as described in Methods. Next, these mice were crossed with mice providing renal epithelial tissue specificity, *Pax8-rtTA*. The resulting mice expressed an optimized reverse tetracyclin-controlled transactivator (rtTA2s-M2) under the control of the Paxillin-8 gene promoter, which permits tissue specific expression of *Cpt1a* gene bearing TRE in proximal and distal tubules and collecting duct after doxycycline administration (**Fig. 1a, b and Supplementary figure 1a, b**). We next characterized the renal specific overexpression of CPT1A in this newly generated genetic mouse model based on the doxycycline inducible transgenic system Tet-On. CPT1A KI mice after doxycycline administration presented a 10-fold increase in CPT1A mRNA level in the whole kidney tissue compared with WT mice **(Fig. 1c**). This was accompanied by a marked augment of CPT1A protein expression in the kidney. Of note, no differences were observed when the liver tissue was analyzed (**Fig.1d, e**). Tubules were labeled by lotus tetragonolobus lectin (LTL), a marker for proximal tubules. Similarly, induced expression of CPT1A and GFP proteins co-localized in tubule segments as evaluated by immunohistochemistry **(Fig. 1f**). Importantly, overexpressed CPT1A presented a mitochondrial localization pattern, which was observed by double immunostaining by using the ATP synthase beta-subunit as a marker (**Fig. 1g**). To assess the magnitude of CPT1A overexpression on FAO, we analyzed the capacity to oxidize radiolabeled palmitate by the renal tissue. Functionally, the increase in CPT1A protein in the renal epithelium increased the capacity of kidney tissue to oxidize ^{14}C-palmitate as reflected in the levels of both ^{14}C-palmitate-derived $^{14}CO_2$ as well as in ^{14}C-palmitate-derived acid-soluble products (**Fig. 1h**).

To evaluate the effect of the Cpt1a knock-in strategy on renal damage we first used the folic acid-nephropathy (FAN) injury model. Folic acid (FA) at high dosage induces the formation of crystals rapidly with tubular necrosis in the acute phase (1–14 days) and patchy interstitial fibrosis in the chronic phase (28–42 days). FAN is induced both by crystal obstruction and direct toxic effect to tubular epithelial cells. Animals were treated with doxycycline starting three weeks prior to FA injection. Histological parameters were evaluated in tissue samples from mice seven days after intraperitoneal (IP) injection of FA. Tubular atrophy and dilation were significantly attenuated and fibrosis was markedly ameliorated in Pax8-rtTAtg/0:tetO-Cpt1atg/0 compared with WT mice (**Fig. 2a, left panel and Supplementary figure 2a, b and c**). A significant reduction in the proportion of fibrosis as quantified by Sirius red was observed in the CPT1A KI model (**Fig.2a, right panel**). Renal function was reduced in FAN-treated WT animals, as reflected by the increase in blood urea nitrogen (BUN) and creatinine, but this effect was blunted in mice overexpressing CPT1A (**Fig. 2b, c**). The protein expression of classical profibrotic markers, fibronectin (FN) and smooth muscle actin (aSMA) was also significantly reduced in the CPT1A KI mice (**Fig. 2d, e**). To confirm the beneficial effect of FAO-gain-of-function in kidney fibrosis, the latter was assessed by performing unilateral ureteral obstruction (UUO) for 3 and 7 days in mice overexpressing CPT1A in TECs. In this model, renal blood flow and glomerular filtration rate in the affected kidney are significantly reduced within 24 h, interstitial inflammation is maximal at 2–3 days while tubular dilation, tubular atrophy and fibrosis are evident after 7 days. Obstructed kidneys from WT animals showed significant tubulo-interstitial architectural and histological changes 7 days after UUO, while the extent of tubular atrophy and dilatation was markedly reduced in kidneys with increased levels of CPT1A **(Supplementary figure 3a, left panel)**. To determine the effect of CPT1A on fibrosis, Sirius red staining was performed to quantify the collagen content in the kidneys. Evaluation of renal lesions by light microscopy showed increased collagen deposition in the interstitial area after 7 days of the procedure in the

obstructed kidneys compared to the contralateral ones in WT mice. A significant protective effect of CPT1A overexpression was observed by a reduction of 20-40% in the collagen deposition (**Supplementary figure 3a, right panel**). As expected, circulating levels of BUN and creatinine were not different between WT and *Cpt1a* knock-in mice after 7 days of UUO due to the remaining functional kidney (**Supplementary figure 3b, c**). A less dramatic but still significant decrease in FN and αSMA was also observed (**Supplementary figure 3d**).

To understand the mechanisms underlying the protective action of CPT1A on renal fibrosis, we performed expression analysis of whole kidney from WT or CPT1A KI mice subjected to FAN or 7-days UUO. Expression of genes related to critical cellular functions for the initiation and perpetuation of tubular dysfunction and chronic tissue damage was analyzed by using specific TaqMan probes. A reduced expression for this subset of genes was observed in the FAN model. QRT-PCR-based quantification displayed lower expression of epithelial injury (*Havcr1*-Kim-1) and fibrotic markers (collagens) in kidneys from CPT1A KI mice (**Fig. 2f**). These data were confirmed by mRNA quantitative analysis using Sybr green (**Supplementary figure 4a**). A similar effect was observed in the UUO model (**Supplementary figure 3e and Supplementary figure 4b**). These observations were also confirmed in the CKD mouse model of adenine-induced nephrotoxicity (ADN). CPT1A KI mice showed a reduction in the induction in the expression of the crucial genes *Col1a1*, *Fn1* and *TGF-β* involved in these cellular mechanisms related to kidney fibrosis (**Supplementary figure 5a, b**). Data collected from the three models of CKD in the CPT1A KI mice strongly support that CPT1A is an enzyme, which, by itself, has a crucial impact on the outcome of fibrosis most likely due to its critical function in the facilitation of FAO.

CPT1A overexpression prevents mitochondrial dysfunction and restores FAO in the fibrotic kidney.

Renal mitochondrial abnormalities and dysfunction are common features in the pathogenesis of different forms of renal disease [5]. Cellular pathways promoting kidney damage can compromise mitochondrial homeostasis reflected in increased oxidative stress, apoptosis, microvascular loss and fibrosis, all of which contribute to renal function deterioration [6]. Thus, we then evaluated morphological alterations of mitochondria in cortical proximal tubules by transmission electron microscopy. Cells from tubular segments of healthy kidneys presented regular apical microvilli, intact basement membrane and basal infoldings. Mitochondria were very abundant; most of them presented an elongated shape and were localized in the basolateral part of the cells. They displayed a well-defined arrangement of well-preserved mitochondrial cisternae with a homogeneous inner matrix. In contrast, in FA-treated mice group, many epithelial cells were detached from the tubular basement membrane and showed disrupted basal infoldings. Mitochondrial structure was lost and mitochondria presented a fragmented, small and round appearance. Interestingly, most of these morphological alterations in mitochondria as well as the reduction in mitochondrial mass induced by FA were almost abrogated in renal epithelial cells overexpressing CPT1A (**Fig. 3a**). In the 3-days UUO and FAN models of kidney damage, CPT1A overexpression prevented the drop of mtDNA copy number (Data not shown and **Fig. 3b**). As previously shown in Fig.1e, the increase in CPT1A protein level in renal epithelium increased the capacity of kidney tissue to oxidize ^{14}C-palmitate by 1.5-fold reflected in the quantity of both ^{14}C-palmitate-derived $^{14}CO_2$ and ASP. As expected, defective FAO was observed in fibrotic kidneys from WT mice. However, in the 3-days UUO, FAN and ADN models, CPT1A overexpression counteracted this impairment, maintaining a FAO rate comparable to healthy kidneys (**Fig. 3c and Supplementary figures 6a and 6c**). Closely related to the improvement in FAO by CPT1A, ATP content in whole kidney tissue increased from 50 to 80 µM/mg protein after CPT1A overexpression. In the 3-days UUO, FAN and ADN models, CPT1A overexpression rescued the drop in ATP levels (**Fig.3d and**

Supplementary figures 6b and 6d). These results suggest that appropriate levels of CPT1A and metabolic function are necessary and sufficient to preserve adequate mitochondrial architecture and morphology.

CPT1A gain-of-function results in enhanced FAO-associated respiration of renal tubular epithelial cells even at the expense of glycolysis and AMPK activation.

TECs use glucose for anaerobic glycolysis. Metabolic alterations of these cells during kidney fibrosis not only involve a defect in FAO but also in glucose oxidation [3]. We found that in the FAN model there was a general downregulation trend in the expression of glycolysis-related genes, which was not recovered by CPT1A overexpression (**Fig. 3e**). By contrast, FAN-induced repression in mRNA levels of the peroxisomal/mitochondrial function-related genes *Acox1*, *Cpt2*, *Lrpprc*, *Sdha* and *Tfam* was prevented in kidneys from CPT1A KI mice (**Fig. 3f**). In the UUO model we found that levels of the majority of the analyzed regulators of glucose utilization were not altered in obstructed kidneys compared to contralateral ones. Only the increased expression of *Ldh1* and *Slc2a1* genes induced by UUO was prevented by CPT1A overexpression (**Supplementary figure 6e**). Similarly, CPT1A-gain-of-function did not induce a major shift towards the expression of peroxisome/mitochondrial-related genes in contralateral kidneys (**Supplementary figure 6f**).

To gain insight about quantitative metabolic changes at the cellular level we examined oxygen consumption (OCR) and extracellular acidification rates (ECAR) of primary TECs isolated from kidneys from CPT1A KI mice (**Fig. 4a**). Basal respiration was measured, followed by exposure to oligomycin, an inhibitor of ATP synthase, which allows determining ATP synthesis-coupled respiration and H+ leak. Then, the uncoupler carbonyl FCCP was added to measure the maximal respiratory capacity, followed by the Complex I inhibitor rotenone and complex III inhibitor antimycin A, which permits to estimate non-mitochondrial respiration (see Methods for details). We found that basal and maximum OCRs were

markedly higher when palmitic acid was supplied to TECs, indicating that TECs efficiently metabolize palmitate. The increase in OCR was sensitive to the CPT1 inhibitor Etomoxir, confirming its specificity (**Fig. 4b**). FAO-associated OCR was also higher in primary kidney epithelial cells isolated from CPT1A KI compared to the ones isolated from WT mice (**Fig. 4c**). Cells treated with TGF-β1 had a lower baseline of oxygen consumption levels and showed a reduction in palmitate-induced elevation in OCR, indicating a low activity of fatty acid metabolism. CPT1A overexpression prevented the TGF-β1-induced bioenergetics derangement (**Fig. 4c**). Simultaneously, glycolytic function associated to palmitate consumption was determined by ECAR. Oligomycin-induced blockage of OXPHOS, allows determining the maximum glycolytic capacity. We found that CPT1A overexpression promoted the inhibition of basal glycolytic function both in the presence and absence of TGF-β1 (**Fig. 4d**).

To confirm the metabolic functional consequences of CPT1A overexpression in the human setting, we examined OCR and ECAR in the human tubular epithelial cell line, HKC-8. Adenoviruses carrying CPT1A (AdCPT1A) or GFP (AdGFP) as a negative control were used to infect HKC-8 cells. CPT1A protein levels were 4-fold higher in CPT1A-expressing HKC-8 than in GFP control cells (**Supplementary figure 7a, b**). As expected, we found that the FAO rate was 2-fold higher in AdCPT1A-expressing HKC-8, as confirmed by measurement of 14C-palmitate-derived $^{14}CO_2$ (**Supplementary figure 7c)**. In consistence with our observations in epithelial cells from murine kidneys overexpressing CPT1A, HKC-8 cells transduced with *CPT1A* exhibited a reduced TGF-β1-induced FAO inhibition (**Supplementary figure 7d**) and suppression of glycolysis as reflected by ECAR levels (**Supplementary figure 7e**).

Depressed carbohydrate, amino acid and lipid oxidative pathways have been described in patients and animal models of CKD, leading to energy deprivation [5]. AMPK is a highly conserved sensor of the intracellular metabolic status and plays a critical role in systemic

energy homeostasis. The AMPK pathway is exquisitely sensitive to alterations in the [AMP]/[ATP] ratio and becomes active when this ratio is shifted towards less ATP. AMPK is activated by phosphorylation of its α-subunit residue Thr172 by upstream kinases. As a result, AMPK promotes catabolic pathways to generate more ATP and inhibits anabolic pathways. AMPK activation subsequently leads to acetyl-CoA carboxylase (ACC) inactivation (by phosphorylation of serine residues) and malonyl-CoA decarboxylase (MCD) activation, decreasing malonyl-CoA concentration and hence favoring FAO [7]. To determine if FAO gain of function in kidneys of CPT1A KI mice was associated to changes in AMPK activation as a consequence of increased ATP levels, phosphorylation of AMPK was analyzed by immunoblot. In the FAN model, obstructed kidneys presented increased AMPK phosphorylation protein levels compared with contralateral kidneys. Importantly, increasing CPT1A levels attenuated AMPK phosphorylation in fibrotic kidneys in the FAN model (**Supplementary figure 8a, b)**. The levels of the ACC phosphorylated form changed accordingly. Similar data were obtained in the UUO and adenine models (**Supplementary figure 8c, d and 8e, f**). Overall it appears that increased FAO associated to overexpression of CPT1A improves mitochondrial respiration in the context of reduced glycolysis. Moreover, it is likely that the enhancement of ATP production related to FAO reins in AMPK activation triggered by chronic kidney damage, with independence of the model employed.

Overexpression of CPT1A modifies the cellular inflammatory profile and abrogates TGF-beta associated epithelial cell damage.

Both studies in patients and in animal models show a strong correlation between infiltrated macrophage polarization and the extent of fibrosis [8]. In the FAN model, flow cytometry analysis revealed that CPT1A overexpression reduced the proportion of renal pro-inflammatory M1 subpopulation (**Fig. 5a and 5b**). By contrast, the macrophage subpopulation positive for CD86 (M1) was higher than the positive for CD206 (M2) in fibrotic

kidneys from the 3- and 7-days UUO models, while CPT1A overexpression did not affect this trend (**Supplementary figure 9a, 9b, 9c and 9d**). However, the M2 macrophage subpopulation was increased in fibrotic kidneys from CPT1A KI mice compared with the WT ones after 7 days UUO (**Supplementary figure 9c and 9d**). Infiltration of macrophage subpopulation positive for both CD86 and CD206 (M1/M2) observed in obstructed kidneys from WT mice 3 or 7 days after UUO was also enhanced by CPT1A overexpression (**Supplementary figure 9b and 9d**). In addition, the abundance of this M1 subpopulation was lower in FAN-induced fibrotic kidneys than in UUO-associated ones (**Fig. 5b and Supplementary figure 9b and 9d**). These data suggest that the changes in the degree of macrophage infiltration and relative contributions of macrophage subpopulations are dependent on the model of kidney injury.

Inflammation is a major hallmark of renal fibrosis, especially in early stages [8]. Consistently, kidney infiltration by CD3+ positive T lymphocytes after FAN was reduced in CPT1A KI compared with WT mice (**Supplementary figure 2c, d**). Thus, we analyzed the profile of prototypical molecules related to inflammation in kidneys from mice overexpressing CPT1A in the context of renal damage. In the FAN model we found a lower expression of inflammation-related markers including the cytokines *IL1b*, *IL6* and *Tnfα* (**Fig. 5c)**, in contrast to findings in the 7 days UUO model (**Supplementary figure 9e**). Consistently, cells from kidneys of mice overexpressing CPT1A presented a reduced population of damaged epithelial cells (CD45- EPCAM+ CD24+) [9] compared to those of WT mice in both the FAN and 7-days UUO models (**Figure 6a and 6b and Supplementary figure 10a and 10b**). Moreover, there was also a reduced expression of the apoptotic markers *Apaf1, Bax and Bcl2* (**Fig. 5d**). A similar pattern regarding the expression of apoptotic markers was observed in the 7 days UUO model (**Supplementary figure 9f)**.

Epithelial cell dedifferentiation is a process associated to the transformation of a terminal cellular phenotype into one with relatively higher potential of differentiation into more than one cell type [10]. Direct epithelial damage causes dedifferentiation and upregulation of mediators that may themselves orchestrate pro-inflammatory signaling. This dedifferentiation is characterized by the loss of epithelial markers and acquisition of mesenchymal features, a process known as epithelial-to-mesenchymal transition (EMT) [11], the role of which in kidney fibrosis remains controversial. We studied the expression of E-cadherin, whose loss is considered as a representative feature of EMT, in the setting of CPT1A overexpression and found no significant differences in renal tubular expression in any of the three models employed (**Supplementary figure 11a)**. A similar pattern was observed when further EMT-associated markers were analyzed in the FAN model. Only the EMT-associated increased expression of Snail was prevented in the kidneys of CPT1A KI mice (**Supplementary figure 11b**). We also tested whether enhancing renal epithelial FAO had a protective role in TGF-β-induced transformation of epithelial cells into a cellular fibrotic phenotype. Primary kidney epithelial cells isolated from CPT1A KI mice and treated with TGF-β1 for 48 h showed a marked reduction in the increase of these EMT-associated markers compared to the cells isolated from WT mice (**Supplementary figure 11c**). Consistently, HKC-8 cells transduced with *CPT1A* exhibited a lower expression of collagen (**Supplementary figure 11d**) and fibronectin (**Supplementary figure 11e**). This set of data supports that the protective action of CPT1A in kidney fibrosis operates, at least in part, through the attenuation of TGF-β1-induced tubular epithelial cell transformation.

An increase in plasma acylcarnitines and a reduction of CPT1A levels is present in patients with CKD.

To explore the importance of FAO in a clinical context we analyzed a cohort of 1,506 patients with CKD and diabetes pertaining to the PREDIMED study [12] (see **Supplementary Table 6**

for details). In those where renal function parameters were available (n=686), we determined the levels of acylcarnitines. We found inverse correlation between GFR and short (c2-c7) and medium (c8-c14)-chain acylcarnitine levels (**Fig. 7a, 7b and Supplementary Table 7 and 8**) in patients with a GFR under 60 ml/min. Thus, CKD patients with a higher GFR showed less accumulation of short and medium-chain acylcarnitines (**Fig. 7d, 7e, 7g**) with no correlation in the case of long-chain (c16-c26) acylcarnitines (**Fig. 7c, 7f**). In a different cohort (see **Supplementary Table 9** for details) we found a positive correlation between tubule CPT1A expression levels and eGFR (**Fig. 7h, 7i**) in a RNAseq study from different pathological backgrounds. The degree of fibrosis also correlated significantly with declining CPT1A levels (**Fig. 7j**). The increase in the levels of acylcarnitines and the reduction in the levels of the limiting step enzyme responsible for their metabolism (CPT1A) most likely reflect a decreased FAO capacity associated to CKD. Thus, these results reinforce the relevance of reduced FAO in CKD and support the importance of its gain-of-function to combat kidney fibrosis as demonstrated in our experimental model.

Discussion

Kidney fibrosis is critically linked to metabolic failure in tubular epithelial cells [13]. We demonstrate that genetic gain-of-function of FAO is sufficient to provide significant mitigation of fibrosis development in three different experimental models of chronic kidney damage. This was reflected in a reduction of fibrotic markers, histological improvement and amelioriation of renal function. Slight differences in the magnitude of changes are most likely due to the variation in the intensity of the inflammatory or the fibrotic components among models. While no experimental model recapitulates with close fidelity human CKD, the fact that we found significant correlation between advanced kidney disease and two signatures of FAO reduction (acylcarnitines and CPT1A) in two large patient cohorts attests to the clinical relevance of a FAO-related major metabolic disturbance in human CKD [14].

The high energetic demand of renal tubular epithelial cells, required for their performance of multiple functions related to the homeostasis of the internal milieu, dictates their dependence on an intact mitochondrial function. We show that FAO gain-of-function, attained by overexpressing tubular CPT1A (in both animals and cells) restores mitochondrial mass and architecture, enhances OCR and increases ATP production in conditions of renal damage. This appears to occur at the expense of glycolysis as ECAR is significantly lower under conditions of CPT1A overexpression. The reciprocal regulation between FAO and glycolysis, the Randle cycle [15], has been demonstrated in muscle and heart, although not in the kidney to our knowledge. Alternatively, it is possible that TECs are consuming lactate as the main fuel for gluconeogenesis, a well-known process occurring in the kidney [16]. The fundamental question as to whether metabolism dictates phenotype is in part answered here, as our data support that an increased capacity of the tubular epithelial cell to meet its energy challenges is able to significantly deter the course of kidney fibrosis. Thus, efforts directed at enhancing FAO in the early stages of fibrosis should very likely pay off to combat human CKD.

Materials and Methods

Generation of a transgenic mouse model for inducible Cpt1a gene. Generation of an inducible conditional transgenic mouse model for *Cpt1a* overexpression in the renal epithelium was based on a 2nd generation Tet-On system with site-specific recombination in embryonic stem (ES) cells [17,18]. Mice harboring the transgene of Cpt1a gene under the control of the tetracycline-responsive promoter element (TRE) (tetO-Cpt1a mice) were generated in the transgenic mice core unit from the National Cancer Research Center (CNIO, Spain). Mice were generated by diploid blastocyst injection. Blastocysts were harvested at 3.5 days post coitum from C57/BL6-J strain females. Between 10 and 15 KH2

ES cells were injected per blastocyst. Approximately 30 injected blastocysts were transferred into pseudo-pregnant CD1 strain recipient females (transgenic mice core unit, CNIO, Spain). Chimeras from the litter with a high percentage agouti coat colour (>80%) were then crossed with C57/BL6-J mice to evaluate germline transmission. Next, these mice were crossed with mice providing renal epithelial tissue specificity, Pax8-rtTA (Jackson labs, Bar Harbor, Ma). Male tetO-Cpt1atg/0 mice were bred with Pax8-rtTAtg/0 female mice to generate double heterozygous Pax8-rtTAtg/0:tetO-Cpt1atg/0 mice and their control littermates in a B6N;129Sv mixed genetic background. Extra-renal expression only occurs at the level of the thyroid and this fact does not interfere with any kidney phenotype [19].

Molecular cloning and gene targeting in ES cells. The CPT1A transgene containing the 5'UTR of the Cpt1a gene, the Cpt1a open reading frame (ORF) (Genbank accession number NM_013495.2), the 2A self-cleaving peptide (P2A), the gene encoding for green fluorescent protein (GFP) and the 3´UTR of the Cpt1a gene were cloned into a unique EcoRI site of pBS31 vector (OriGene Technologies, Rockville, Maryland). This vector contains the phosphoglycerate kinase (PGK) promoter followed by an ATG start codon and a FRT recombination site, a splice acceptor-double polyA cassette, the tetracycline operator with a cytomegalovirus (CMV) minimal promoter and an SV40 polyA signal, assembled in Bluescript. By using FRT/flippase-mediated recombination system, which permits the generation of single copy transgenes in predetermined integration sites [17,18], the CPT1A transgene was targeted into the downstream region of the collagen 1a1 (Col1a1) locus of KH2 embryonic stem (ES) cells containing a frt-flanked PGK-neomycin-resistance gene followed by a promoterless, ATG-less hygromycin-resistance gene. These cells also contained the M2-rtTA under control of the endogenous ROSA26 promoter [20]. For gene targeting, 50 µg pBS31 vector and 25 µg vector encoding the flippase (pCAGGS-FLP) [21] were co-electroporated with 1.5 x 107 KH2 ES cells at 400 V and 125 µf using two pulses

in a Gene PulserII (Bio-Rad, Hercules, CA). Recombination between FRT sites such that the entire plasmid is inserted within the PGK promoter and the ATG initiation codon upstream and in frame with the hygromycin resistance gene was used to select correctly targeted cells. ES cells were treated with 140 µg/ml hygromycin B (Carl Roth, Karlsruhe, Germany) after 48 h post electroporation to select clones that had undergone site-specific recombination and individual clones were picked after 8-14 days. Individual ES clones were tested in vitro by treating them with 1µg/ml doxycycline (Sigma, St. Louis, MO) in the culture media for 4 days. Then, GFP was measured in a BD FacsCantoTM II cytometer (BD Bioscience, San José, CA) to assess the electroporation efficiency and cells expressing GFP were sorted. Dox-induced CPT1A was also analyzed by immunoblot as described above.

Doxycycline induction. To induce CPT1A expression, 8-week-old Pax8-rtTAtg/0:tetO-Cpt1atg/0 mice and corresponding Pax8-rtTA0/0:tetO-Cpt1atg/0 (WT) mice were fed with doxycycline (Sigma, St. Louis, MO) at concentrations of 1 mg/ml via drinking water for 3 weeks. Mice were housed in colony cages with a 12:12-h light-dark cycle in a temperature- and humidity-controlled environment with free access to water.

Genotyping. Mice were genotyped by PCR using DNA extracted from tail biopsies and the primers listed in **Supplementary** ¡Error! No se encuentra el origen de la referencia.. DNA extraction was performed by using the AccuStart™ II Mouse Genotyping Kit according to the manufacturer's instructions.

Cell lines and culture conditions. Human proximal tubular epithelial cells (HKC-8) were cultured in DMEM/F12 (Dulbecco's modified Eagle's medium 1:1 (v/v)) (Corning, New York, NY) supplemented with 15 mM Hepes, 5% (vol/vol) fetal bovine serum (FBS) (HyClone

Laboratories, Logan, UT), 1x Insulin-Transferrin-Selenium (ITS) (Gibco, Rockville, MD), 0.5 µg/ml hydrocortisone (Sigma, St. Louis, MO), 50 units/mL penicillin and 50 µg/mL streptomycin (Gibco, Rockville, MD) at 37ºC and 5% CO_2. HEK293A cells were cultured in DMEM supplemented with 10% (v/v) FBS (HyClone Laboratories, Logan, UT) and 1% penicillin /streptomycin (Gibco, Rockville, MD) at 37ºC and 5% CO_2. All cells were treated with trypsin every five days for sub-culturing. Treatments with human recombinant 10 ng/ml TGF-β1 (R&D Systems, Minneapolis, MN) were performed after serum-free starvation of HKC-8 for 12 hours (h). Cells from the embryonic stem cell line KH2 derived from 129/Bl6-J mice were cultured on irradiated murine embryonic fibroblast (MEF) cells according to standard procedures [22]. Briefly, cells were seeded at a density of 3×10^4 cells/cm^2 in DMEM supplemented with leukemia inhibitory factor (LIF) at 1000 units/ml (Corning, New York, NY), 15% ES qualified fetal bovine serum (FBS), non-essential amino acids and sodium pyruvate (Gibco, Rockville, MD) and passaged every day.

Isolation of primary kidney epithelial cells. Kidneys from CPT1A KI and wild-type (WT) mice (3- to 5-week-old males) were collected after sacrifice by cervical dislocation and perfusion with PBS. The capsule was removed and the cortex from 2 kidneys was dissected, placed in 1 mL ice-cold phosphate buffered saline (PBS) (Corning, New York, NY), and minced into pieces of approximately 1 mm^3. These pieces were digested with 10 ml HBSS containing 2 mg/mL collagenase I (Thermo Scientific, Rockford, IL) for 30 minutes at 37°C with gentle stirring and supernatants were sieved through a 100-µm nylon mesh. After centrifugation for 10 minutes at 3000 rpm, the pellet was resuspended in sterile red blood cell lysis buffer (8.26 g NH4Cl, 1 g KHCO3, and 0.037 g EDTA per 1 L ddH2O) and seeded in 10-cm culture dishes. Cells were cultured in RPMI 1640 (Corning, New York, NY) supplemented with 10% FBS (HyClone Laboratories, Logan, UT), 20 ng/mL EGF (Sigma, St. Louis, MO), 20 ng/ml bFGF (Sigma, St. Louis, MO), 50 units/mL penicillin and 50 µg/mL streptomycin (Gibco,

Rockville, MD) at 37ºC and 5% CO_2. Media were changed 24 hours after plating and every 48–72 hours thereafter. Cells were used between days 7 and 10 of culture. Treatments (10 ng/ml) with human recombinant TGF-β1 (R&D Systems, Minneapolis, MN) were performed after serum-free starvation of cells for 12 h.

Transfection procedure. Cells were seeded into 60 mm culture dishes to reach a confluence of 70%. They were transfected with 40 nM of either mirVana™ miRNA mimic of miR-150, miR-495 or miR-33, miR-33 inhibitor or mirVana™ miRNA mimic/inhibitor negative control (Ambion company, USA) using lipofectamine 2000 (Invitrogen, Carlsbad, CA). Cells were incubated with the lipofectamine-pre-miRNA 37 °C for 6 h. Subsequently, 5 ml fresh medium containing 10% FBS were added to the culture dishes and the cells were maintained in culture until used for subsequent experiments.

Immunoblot. Cells were washed in PBS, homogenized and lysed in 100 µL RIPA lysis buffer containing 150 mM NaCl, 0.1% SDS, 1% sodium deoxycholate, 1% NP-40 and 25 mM Tris–HCl pH 7.6, in the presence of protease (Complete, Roche Diagnostics, Mannheim, Germany) and phosphatase inhibitors (Sigma-Aldrich, St. Louis, MO) and harvested by scraping. A quarter piece of each kidney sample (obtained after dissection in half both lengthwise and crosswise) was homogenized in 300 µl RIPA buffer above described with 5 mm stainless steel beads (Qiagen, Valencia, CA) using TissueLyser LT (Qiagen, Valencia, CA) vibrating at 50 Hz for 15 min at 4°C. Samples were clarified by centrifugation at 10,000 g for 15 min at 4°C. The pellet was then discarded, and the supernatant was kept as protein lysate. Protein concentrations were determined by the BCA Protein Assay Kit (Thermo Scientific, Rockford, IL) and was measured in Glomax®-Multi Detection system (Promega, Madison, WI). Equal amounts of protein (10–50 µg) from the total extract were separated on 8–10% SDS–polyacrylamide gels and transferred onto nitrocellulose blotting membranes

(GE Healthcare, Chicago, IL) at 12 V for 20 min in a semi-dry Trans-Blot Turbo system (Bio-Rad, Hercules, California). Membranes were blocked by incubation for 1 h with 5% non-fat milk in PBS containing 0.5% Tween-20 and blotted overnight with the specific antibodies listed in **Supplementary** ¡Error! No se encuentra el origen de la referencia.. After incubation with IRDye 800 goat anti-rabbit and IRDye 600 goat anti-mouse (1:15,000, LI-COR Biosciences, Lincoln, NE) secondary antibodies, membranes were imaged in triplicates with the Odyssey Infrared Imaging System (LI-COR Biosciences, Lincoln, NE). Band densitometry was performed using the ImageJ 1.48 software (http://rsb.info.nih.gov/ij) and relative protein expression was determined by normalizing to GAPDH. Fold changes were normalized to values of control condition.

RNA extraction. Total RNA was extracted from HKC-8 or mouse kidneys using the miRNeasy Mini Kit (Qiagen, Valencia, CA) according to the manufacturer's instructions. RNA quantity and quality were determined at 260 nm by a Nanodrop-1000 spectrophotometer (Thermo Scientific, Rockford, IL).

Analysis of mRNA expression. Reverse transcription (RT) was carried out with 500 ng of total RNA using the iScript™ cDNA Synthesis kit (Bio-Rad, Hercules, CA). qRT–PCR was carried out with the iQ™SYBR Green Supermix (Bio-Rad, Hercules, CA), using a 96-well Bio-Rad CFX96 RT–PCR System with a C1000 Thermal Cycler (Bio-Rad, Hercules, CA) according to the manufacturers' instructions. A C_t value was obtained from each amplification curve using CFX96 analysis software provided by the manufacturer. Relative mRNA expression was determined using the $2^{-\Delta\Delta Ct}$ method [23]. The 18S gene was used for normalization purposes. The primer sequences used for mRNA quantification are listed in **Supplementary Table 3**. Fold changes were normalized to values of control condition.

Mouse models of kidney fibrosis. Mice were housed in the Specific-pathogen-free (SPF) animal facility at the CBMSO in accordance with EU regulations for all the procedures. Animals were handled in agreement with the Guide for the Care and Use of Laboratory Animals contained in Directive 2010/63/EU of the European Parliament. Approval was granted by the local ethics review board of the Centro de Biología Molecular "Severo Ochoa" in Madrid, the Ethics committee at CSIC and the Regulatory Unit for Animal Experimental Procedures from the Comunidad de Madrid.

Unilateral ureteral obstruction (UUO). UUO surgery procedure was performed as previously described [24]. Briefly, mice were anesthetized with isofluorane (3-5% for induction and 1-3% for maintenance) and divided into two experimental groups: the UUO group and the sham operation group. In the UUO group, mice were shaved on the left side of the abdomen, a vertical incision was made through the skin with a scalpel and the skin was retracted. A second incision was made through the peritoneum to expose the kidney. The left ureter was ligated twice 15 mm below the renal pelvis with surgical silk and the ureter was then severed between the two ligatures. Then, the ligated kidney was placed gently back into its correct anatomical position and sterile saline was added to replenish loss of fluid. The incisions were sutured and mice were individually caged. The sham operation was performed in a similar manner, but without ureteral ligation. Buprenorphine was used as an analgesic. A first dose was administered 30 minutes before surgery and then every 12 hours for 72 hours, at a dose of 0.05 mg / kg subcutaneously. In this model, renal blood flow and glomerular filtration rate become significantly reduced within 24 h and interstitial inflammation (peak at 2–3 days), tubular dilation, tubular atrophy and fibrosis are evident after 7 days. The obstructed kidney reaches maximal dysfunction around 2 weeks after the procedure. Mice were sacrificed by CO_2 overdose and control and obstructed kidney and blood samples were harvested after perfusion with PBS at 3 and 7 days after UUO.

Folic acid-induced nephropathy (FAN). In this model, kidney fibrosis was induced by intraperitoneal (i.p) injection with 250 mg folic acid (Sigma-Aldrich, St. Louis, MO) per kg body weight dissolved in 0.3 M sodium bicarbonate (vehicle) as previously described [25]. Control animals received 0.3 ml of vehicle (i.p). Mice were sacrificed by CO2 overdose and kidneys and blood samples were harvested after perfusion with PBS after 15 days of FA administration.

Adenine-induced renal failure (ADN). Adenine (Sigma-Aldrich, St. Louis, MO) was administered daily to mice at 50 mg/kg body weight in 0.5% carboxymethyl cellulose (CMC) (Wako Pure Chemical Industries Ltd., Osaka, Japan) by oral gavage for 28 days as previously described [26]. Control animals received daily 0.5% CMC administered by oral gavage for the same period of time. Mice were sacrificed by CO_2 overdose and kidneys and blood samples were harvested after perfusion with PBS after 28 days of the first adenine dose administration.

[1-14C] Palmitate oxidation. Measurement of fatty acid oxidation (FAO) rates was performed in mouse kidney tissue and cells as previously described [27]. Kidneys from renal fibrosis mouse models were decapsulated, diced and then homogenized in 5 volumes of chilled STE buffer by a Dounce homogenizer. Crude homogenates were centrifuged at 420 g for 10 min at 4 °C. Thirty µL of tissue homogenate supernatant was mixed with 370 µL of the oxidation reaction mixture containing 7% BSA/5 mM palmitate/0.01 µCi/µL ^{14}C-palmitate (PerkinElmer, Waltham, MA) and incubated at 37 °C for 30 min. In the case of cells, they were seeded in 12-well dishes to reach a confluence of 70% and were infected with CPT1A adenoviruses as described in the adenovirus-mediated CPT1A overexpression procedure section. Then, cells were incubated in 500 µL of media containing 0.3% BSA/100 µM

palmitate/0.4 µCi/mL ^{14}C-palmitate at 37 °C for 3 h. Each sample was assayed in triplicate. The reaction was stopped by the addition of 200 µl of 1 M perchloric acid. The rate of palmitate oxidation was measured as released $^{14}CO_2$ trapped in a filter paper disk with 20 µL of 1 M NaOH in the top of sealed vials. $^{14}CO_2$ traps were transferred to scintillation vials to determine ^{14}C-palmitate-derived $^{14}CO_2$. The remaining acid solution for each sample was centrifuged at 14,000 g for 10 min at 4 °C and 400 µL of supernatant was also added to scintillation vials for the quantification of ^{14}C-palmitate-derived acid-soluble metabolites. Control incubations without cells or tissue samples were also run in parallel. ^{14}C products were counted in an LS6500 liquid scintillation counter (Beckman Instruments Inc., Brea, CA). Scintillation values were converted to mmol $^{14}CO_2$ or acid-soluble metabolites multiplying the specific activity and normalized to the protein content.

TaqMan gene expression assay. TaqMan Array Plates (Thermo Scientific, Rockford, IL) were selected as the platform for gene expression profiling. This panel consisted of a total of 43 unique TaqMan probes specific for mouse gene related with fibrosis, apoptosis, mitochondrial metabolism, glucose utilization and inflammation listed in **Supplementary Table 4**. RNA from kidney samples was performed as described in the RNA extraction procedure section. Two µg of total RNA were subjected to reverse transcription using High-Capacity cDNA Reverse Transcription Kit (Thermo Scientific, Rockford, IL) according to the manufacturer's instructions. PCR amplification was performed using TaqMan® master (Thermo Scientific, Rockford, IL) with the Roche LightCycler 480 Real-Time PCR system (AB7900HT). This procedure was performed in the Genomic Facility of the Fundación Parque Científico de Madrid (Madrid, Spain). The ABI TaqMan SDS v2.4 software was utilized to obtain Cq values (Cq) for each gene. The Cq data were analyzed with the StatMiner 4.2.8 software (Integromics; Madrid, Spain). The delta C_t (ΔCt) value was calculated by normalizing C_t values to the endogenous housekeeping 18S. Relative mRNA

expression was determined using the $2^{-\Delta\Delta Ct}$ method [23]. Fold changes were normalized to values of control condition.

Mitochondrial copy number determination. Genomic DNA was extracted from mouse kidneys using the DNeasy Blood & Tissue Kit (Qiagen, Valencia, CA) according to the manufacturer's instructions. DNA quantity and quality were determined at 260 nm by a Nanodrop-1000 spectrophotometer (Thermo Scientific, Rockford, IL). Mitochondrial abundance was determined with the Mouse Mitochondrial DNA Copy Number Assay Kit (Detroit R&D, Detroit, MI). Relative mtDNA copy number was presented as the mtDNA-to-nuclear DNA ratio.

Assessment of kidney function. Animal kidney function was determined by analyzing the indicators, serum creatinine and Blood Urea Nitrogen (BUN). They were analyzing by using the QuantiChrom TM Creatinine Assay Kit (Bioassay systems, Hayward, CA) and the Blood Urea Nitrogen (BUN) Colorimetric Detection Kit (Ann Arbor, MI), respectively, according to the manufacturers' instructions. Serum was obtained from blood samples by centrifugation at 3000 rpm for 15 min.

Quantification of kidney cell populations by flow cytometry. Multiparametric flow cytometry was used for the identification of macrophage and epithelial cell population. Kidneys were decapsulated, diced, then incubated at 37ºC for 30 min with 0.5 mg/ml liberase DL (Roche Basel, Switzerland) and 100 U/ml DNase (Roche Basel, Switzerland) in serum free DMEM. After centrifugation (10 min, 2500 rpm at 4ºC), cells were resuspended in 5ml of buffer (1% BSA and 1% FBS in PBS) and filtered (40µm). For staining, 10^6 cells were dissolved in 50 µl of buffer and pre-incubated with 0.25µl CD16/CD32 (BioLegend, San Diego, CA) to block interactions with the Fc domain of immunoglobulins. Three µl of 4,6-diamidino-2-

phenylindole (DAPI) (1:15000) (Sigma, St. Louis, MO) was added to stain dead cells. Cell suspensions were incubated with specific fluorochrome-conjugated antibodies (BioLegend, San Diego, CA) listed in **Supplementary Table 5**. For each experiment, flow minus one (FMO) controls was performed for each fluorophore to establish gates by using corresponding antibodies listed in **Supplementary Table 5**. Fluorescence intensity was measured in a BD FacsCantoTM II cytometer (BD Bioscience, San José, CA) and analyzed with the FlowJo 10.2 software (FlowJo, LLC, Ashland, OR). For each kidney sample, at least 20,000 singlets were analyzed in triplicates. Negative gates were set to exclude other cell types from the positive selection by using appropriate isotype control antibodies. Cell gating was initially based in the Forward versus Side scatter (FSC vs SSC) plot. Next, dead cells were excluded. Identification of the macrophage cell population was based on the presence of CD45, expressed in inflammatory and hematopoietic cells and F4/80, a specific macrophage surface marker. CD86 and CD206 were used to determine M1 and M2 macrophage subpopulations, respectively [28]. Identification of the epithelial cell population was based on the presence of the epithelial cell adhesion molecule (EpCAM) and the absence of CD45. The subsequent display of positive CD24 determined injured proximal tubule epithelia [29]. Numbers in quadrants indicate cell proportions in percent of cells that co-express both markers.

Measurements of oxygen consumption rate. Fatty acid oxidation-associated oxygen consumption rate (OCR) (ligated to oxidative phosphorylation) and extracellular acidification rate (ECAR) (associated with lactate production and glycolysis) were studied using the Seahorse Bioscience metabolic analyzer according to the manufacturer's instructions [30]. HKC-8 cells were seeded in a p60 plate and microRNA transfection or adenovirus-mediated CPT1A overexpression was performed (as shown in the transfection procedure and adenovirus-mediated overexpression sections, respectively) when they reached a

confluence of 70% and 48 hours later, HKC-8 cells were treated with 10 ng/ml TGF-β1 for 48 h. In the case of primary kidney epithelial cells, they were seeded in a p60 plate and when they reached a confluence of 70%, they were treated with 10 ng/ml TGF-β1 for 48 h. In all cases, cells were then seeded at 2×10^4 cells per well in a Seahorse Bioscience XFe24 cell culture microplate (Seahorse Bioscience, North Billerica, MA). After cell adherence, growth medium was replaced with substrate-limited medium, Dulbecco's Modified Eagle Medium (DMEM) supplemented with 0.5 mM Glucose and 1 mM Glutamate. One hour before the assay measurement, cells were incubated with Krebs-Henseleit Buffer (KHB) assay medium supplemented with 0.2% carnitine at 37ºC without CO2. Fifteen minutes before the assay, the CPT1 inhibitor Etomoxir (Eto) (Sigma-Aldrich, St. Louis, MO) 400 μM was added to the corresponding wells and cells were incubated at 37ºC without CO2. Finally, just before starting the assay, BSA or 200 μM Palmitate-BSA FAO Substrate (Agilent Technology, Santa Clara, CA, USA) was added. Immediately, XF Cell Mito Stress Test was performed in a Seahorse XFe24 energy analyzer by adding sequentially during the assay several modulators of mitochondrial function. First the ATP synthase inhibitor oligomycin (Sigma-Aldrich, St. Louis, MO) (1 μM) was used following basal measurement. This decreases electron flow through the ETC, resulting in a reduction in mitochondrial respiration. Next, the uncoupling agent cyanide 4-(trifluoromethoxy) phenylhydrazone (FCCP) (Sigma-Aldrich, St. Louis, MO) (3 μM), that collapses the proton gradient and disrupts the mitochondrial membrane potential was added. As a result, electron flow through the ETC is uninhibited, and oxygen consumption by complex IV reaches its maximum. The third and last injection is a mixture of the complex III and I inhibitors antimycin/rotenone (Sigma-Aldrich, St. Louis, MO) (1 μM). This combination shuts down mitochondrial respiration and enables the calculation of non-mitochondrial respiration driven by processes outside the mitochondria. Substrates/inhibitors were prepared in the same medium in which the experiment was conducted and were injected from the reagent ports automatically at the

times indicated. Measurements were registered for 3-minute periods of time (over a total period of 2 hours) and values were normalized for total protein content. Protein was extracted from wells with 0.1% NP-40-PBS solution, and quantified with BCA protein assay (Thermo Scientific, Rockford, IL). Four wells were used for each experimental group. Basal mitochondrial respiration, ATP-linked respiration, proton leak (non-ATP–linked oxygen consumption), maximal respiration, non-mitochondrial respiration and reserve respiratory capacity were determined as described [31].

Immunofluorescence. A quarter piece of each kidney sample (obtained after dissection in half both lengthwise and crosswise) was immersed sequentially in 4% neutral buffered formalin for 24 hous, in 30% sucrose in PBS until tissue sank (6-12 h) and embedded in Tissue-Tek® OCT for cryoprotection at -80ºC. OCT blocks were cut in serial frozen sections (10µm thickness). These sections were fixed with 4% PFA for 10 min and permeabilized with 0.25% Triton X-100 in PBS for 5 min at room temperature (RT). Next, they were washed with PBS, blocked with 1% BSA in PBS for 30 min at RT and incubated for 1 h for staining with specific primary antibodies: anti-CPT1A antibody (1:1000, ab128568, Abcam, Cambridge, UK), biotinylated lotus tetragonolobus lectin (LTL) (1:1000, B-1325, Vector Laboratory, (Burlingame, CA) anti-β-F1-ATPase (clone 11/21-7 A8, 1: 1.000), kindly provided by Dr. Jose Manuel Cuezva (UAM, Madrid, Spain) [32]. Subsequently, sections were washed with PBS incubated with the corresponding fluorochrome-conjugated secondary antibodies: Alexa Fluor 555 anti-Mouse antibody (1:1000, A-21137, Thermo Scientific, Rockford, IL), (1:1000, A-21206, Thermo Scientific, Rockford, IL), Streptavidin Alexa Fluor™ 555 Conjugate (1:400, S32355, Thermo Scientific, Rockford, IL), respectively for 1h at RT. Nuclei were stained with DAPI (Sigma, St. Louis, MO) for 5 min at RT. The coverslips were mounted on slides using mowiol (Calbiochem). Tissue fluorescence was visualized by a

LSM 510 Meta Confocal microscope with a 40X/1.3 oil Plan-Neofluar M27 objective (Zeiss, Oberkochen, Germany).

Histological and immunohistochemical analysis. A quarter piece of each kidney sample (obtained after dissection in half both lengthwise and crosswise) was immersed in 4% neutral buffered formalin for 24 hous, embedded in paraffin, cut in serial sections (5µm thickness) and stained with hematoxylin and eosin (H&E), Sirius red and periodic acid-schiff (PAS) stainings as described previously [33]. H&E and Sirius red stainings were performed in the histology facility of the National Center of Biotechnology (Madrid, Spain). Immunostaining was carried out in 4-µm-thick tissue sections that were deparafinized through xylene and hydrated through graded ethanol (100%, 96%, 90%, and 70%) and distilled water. Endogenous peroxidase was blocked. We incubated the tissue sections with 4% BSA for 1 h at room temperature and serum in 1× PBS to eliminate nonspecific protein binding sites. Primary antibodies to detect CD3 (M7254, 1:100, Dako, Spain) were incubated for 30 minutes at room temperature. After washing, slides were incubated with goat anti-mouse HRP secondary antibody ("Visualization Reagent HRP" from SK006, Dako, Spain) for 30 min and visualized using the PD-L1 IHC 22C3 pharmDx (SK006, Dako, Spain). To detect Kim-1, primary antibodies (AF1817, 1:500, RyD Systems, Minneapolis, MN) were incubated for 30 minutes at room temperature. After washing, slides were incubated with goat anti-rabbit IgG biotin-SP conjugate secondary antibody (31752, 1:200, Invitrogen, Carlsbad, CA) and visualized using DAB Substrate Kit (ab64238, abcam, Abcam, Cambridge, UK). Tissue sections were revealed using 3,3'-diaminobenzidine (20 µl/ml, DAB, Dako, Spain) as chromogen and counterstained with Carazzi's hematoxylin. Negative controls included non-specific immunoglobulin and no primary antibody. Slides were mounted with mowiol (Merck Millipore, Germany). Fibrosis was quantified in Sirius red-stained sections in order to detect collagen fibers. The area of interstitial fibrosis was

identified, after excluding the vessel area from the region of interest, as the ratio of interstitial fibrosis or collagen deposition to total tissue area and expressed as %FA (fibrotic area). Tubular atrophy and tubular dilation were evaluated as previously described in PAS-stained sections [34]. Renal T lymphocyte infiltration was quantified by CD3 stained area versus total analyzed area. For each kidney, 10–15 fields were analyzed with a 40X objective lens under transmitted light microscopy by using a digital camera (Nikon D3) connected to a Nikon's Eclipse TE2000-U light microscope (Nikon Instruments Europe B.V., Badhoevedorp, The Netherlands). Intensity measurements of Sirius red and CD3 staining area were performed blind in an automated mode using the ImageJ 1.48 software (http://rsb.info.nih.gov/ij). Furthermore, qualitative evaluation of the tissue was performed by a renal pathologist in a blinded fashion.

Electron microscopy examination. The number of mitochondria and their structure was analyzed by standard transmission electron microscopy. Renal cortex pieces were cut into small blocks (1 mm^3) and fixed by immersion in fixative (4% paraformaldehyde/2% glutaraldehyde in 0.1 M phosphate buffer) for overnight at 4ºC. After washing with cold PBS and incubated in 1% osmium tetroxide and 1% potassium ferricyanide in water for 1 hour at 4ºC. Pieces were sequentially stained with 0.15% tannic acid (in 0.1 M phosphate buffer) for 1 min at room temperature (RT), and 2% uranyl acetate in water for 1 hore at RT. Next, they were dehydrated in graded ethanol, and embedded in EmBed812 resin (Electron Microscopy Sciences, Fort Washington, PA). Serial ultrathin sections (70 nm) of the tissue were collected on copper mesh grids. Three grids from each sample were examined using a JEOL 1230 transmission electron microscope, and digital photographs were captured by real-time digital imaging.

Measurements of oxygen consumption rate. Fatty acid oxidation-associated oxygen consumption rate (OCR) (ligated to oxidative phosphorylation) and extracellular acidification rate (ECAR) (associated with lactate production and glycolysis) were studied using the Seahorse Bioscience metabolic analyzer according to the manufacturer's instructions [30]. HKC-8 cells were seeded in a p60 plate and microRNA transfection or adenovirus-mediated CPT1A overexpression was performed (as shown in the transfection procedure and adenovirus-mediated overexpression sections, respectively) when they reached a confluence of 70% and 48 hours later, HKC-8 cells were treated with 10 ng/ml TGF-β1 for 48 h. In the case of primary kidney epithelial cells, they were seeded in a p60 plate and when they reached a confluence of 70%, they were treated with 10 ng/ml TGF-β1 for 48 h. In all cases, cells were then seeded at 2×10^4 cells per well in a Seahorse Bioscience XFe24 cell culture microplate (Seahorse Bioscience, North Billerica, MA). After cell adherence, growth medium was replaced with substrate-limited medium, Dulbecco's Modified Eagle Medium (DMEM) supplemented with 0.5 mM Glucose and 1 mM Glutamate. One hour before the assay measurement, cells were incubated with Krebs-Henseleit Buffer (KHB) assay medium supplemented with 0.2% carnitine at 37ºC without CO2. Fifteen minutes before the assay, the CPT1 inhibitor Etomoxir (Eto) (Sigma-Aldrich, St. Louis, MO) 400 µM was added to the corresponding wells and cells were incubated at 37ºC without CO_2. Finally, just before starting the assay, BSA or 200 µM Palmitate-BSA FAO Substrate (Agilent Technology, Santa Clara, CA, USA) was added. Immediately, XF Cell Mito Stress Test was performed in a Seahorse XFe24 energy analyzer by adding sequentially during the assay several modulators of mitochondrial function. First the ATP synthase inhibitor oligomycin (Sigma-Aldrich, St. Louis, MO) (1 µM) was used following basal measurement. This decreases electron flow through the ETC, resulting in a reduction in mitochondrial respiration. Next, the uncoupling agent cyanide 4-(trifluoromethoxy) phenylhydrazone (FCCP) (Sigma-Aldrich, St. Louis, MO) (3 µM), that collapses the proton gradient and

disrupts the mitochondrial membrane potential was added. As a result, electron flow through the ETC is uninhibited, and oxygen consumption by complex IV reaches its maximum. The third and last injection is a mixture of the complex III and I inhibitors antimycin/rotenone (Sigma-Aldrich, St. Louis, MO) (1 μM). This combination shuts down mitochondrial respiration and enables the calculation of non-mitochondrial respiration driven by processes outside the mitochondria. Substrates/inhibitors were prepared in the same medium in which the experiment was conducted and were injected from the reagent ports automatically at the times indicated. Measurements were registered for 3-minute periods of time (over a total period of 2 hours) and values were normalized for total protein content. Protein was extracted from wells with 0.1% NP-40-PBS solution, and quantified with BCA protein assay (Thermo Scientific, Rockford, IL). Four wells were used for each experimental group. Basal mitochondrial respiration, ATP-linked respiration, proton leak (non-ATP–linked oxygen consumption), maximal respiration, non-mitochondrial respiration and reserve respiratory capacity were determined as described [31].

Adenovirus-mediated CPT1A overexpression. CPT1A overexpression in cells was driven and transduced by adenoviral particles. Adenoviruses carrying GFP (AdGFP) and CPT1A (AdCPT1A) were amplified, purified and titrated according to [35]. Briefly, adenovirus production consisted of two rounds of amplification. In the first amplification round, HEK293A cells in a 100 cm^2 dish at 70% confluence growing in complete medium supplemented with 5% of FBS (infection media) were infected with 50 μl of the adenovirus stock, while in the second amplification round, 10 X 100 cm^2 dishes of 70% confluent HEK293A cells /virus type were infected with 400 μl of the first amplification of the adenovirus. After 20 h, cells from all dishes were harvested together by scraping and centrifuged (1,000 rpm for 5 min at 4ºC). The cell pellet was disrupted by 3 cycles of freeze and thaw using liquid N_2 and resuspended in 5 mL of infection media. Cell debris was discarded by centrifugation at 3,000

rpm for 10 min at 4ºC and supernatant containing adenoviruses was stored in 500 µl aliquots to be used throughout the experiments. Titration was performed by using the Adeno-X™ Rapid Titer Kit (Clontech Laboratories, Palo Alto, CA) according to the manufacturer's instructions, which is based on the antibody specific detection of the adenoviral hexon protein by peroxidase (HRP). HCK8 cells were seeded into 60 mm culture dishes to reach a confluence of 70%. They were infected with adenoviruses AdGFP and AdCPT1A [100 moi (multiplicity of infection)] for 24 h in serum-free DMEM/F12 (supplemented with 15 mM Hepes, 5% FBS, 1x ITS, 0.5 µg/ml hydrocortisone, 50 units/mL penicillin and 50 µg/mL streptomycin) and then the medium was replaced with complete medium for additional 24 h. Adenovirus infection efficiency was assessed in AdGFP-infected cells by immunofluorescence.

Clinical data. Acylcarnitines were evaluated based on the PREDIMED trial. The PREDIMED is a primary prevention multicenter trial conducted in Spain. A detailed description of this trial is described elsewhere [12]. Liquid chromatography–tandem mass spectrometry was used to semi-quantitatively profile acylcarnitines in plasma samples. Our analysis is based on a subsample of 686 participants with metabolomics data and measures of kidney function including glomerular filtration rate and urinary albumin-creatinine ratio [36]. Studies of CPT1A expression in kidney tubules were performed in a cohort of 433 patients (described in [37] and hereon named CKD cohort), whose demographic and clinical features are summarized in **Supplementary table 9**.

Statistical analysis. Data in experimental models were analyzed using nonparametric tests except where indicated. The difference between two independent groups was examined with Mann-Whitney test, while more than two groups were compared with Kruskal-Wallis test. A P-value of 0.05 or less was considered statistically significant ($^{*/\#}$: $P < 0.05$, $^{**/\#\#}$: $P < 0.01$, $^{***/\#\#\#}$: $P < 0.001$). Data were analyzed using GraphPad Prism 6.0 (GraphPad Software, La Jolla, CA). Data are reported as mean ± standard error of mean (SEM).

Data in clinical studies for acylcarnitines: Means and standard deviations (SD) were used to describe continuous variables and percentage to describe categorical values. Metabolite measures were normalized using a logarithmic transformation and scaled to multiples of SD using z-score standardization. Three scores were created according to the number of carbons: short (2-7), medium (8-14) and long (16-26) acylcarnitine scores. The sum of the log-transformed values of each carnitine was computed to calculate these scores and a z-score standardization was also applied. Chi-squared and Student´s t-test were used to compare categorical and quantitative variables, respectively. Univariate and multivariable linear regression models were conducted to assess the association between the glomerular filtration rate (GFR) and both the acylcarnitine scores and individual metabolites. The covariates used in the multivariable models were age, sex, type-2 diabetes and albumin/creatinine ratio.

Data in clinical studies for CPT1A expression: ANOVA test was performed to assess the significance across different disease groups and cor.test() function in R was used to get the Pearson's correlation and the corresponding P-values.

Author contributions

SL conceived and directed research. VM designed, performed and analyzed the majority of experiments. JT and LME performed experiments. JIH provided technical assistance for mouse experiments. CC performed histological evaluation. LH and DS provided the CPT1A

adenoviruses. MRO, DRP, PC and CB provided intellectual and technical insight. RR assisted with the Taqman analysis. SO coordinated the generation of the CPT1A KI mouse model. XS, KS, MRC, JSS, FBH and MAMG performed studies in two different cohorts of CKD patients. All authors helped with the discussion of the results and SL and VM wrote the manuscript.

Acknowledgements

This work was supported by Grants from the Ministerio de Economía y Competitividad (MINECO) SAF2012-31388 (SL), SAF2015-66107-R (SL), PI17/01513 (DRP), SAF2017-83813-C3-1-R (DS and LH) cofunded by the European Regional Development Fund, Instituto de Salud Carlos III REDinREN RD12/0021/0009 and RD16/0009/0016 (SL, DRP and MRO), PI17/00119 (MRO), FIS PI17/00625 (DRP), Comunidad de Madrid "NOVELREN" B2017/BMD-3751 (SL, DRP and MRO), a grant-in-aid from the Spanish Society of Nephrology (Fundación Senefro 2017) to SL and Fundación Renal "Iñigo Alvarez de Toledo" (SL), the Centro de Investigación Biomédica en Red de Fisiopatología de la Obesidad y la Nutrición (CIBEROBN) CB06/03/0001 (DS), the Government of Catalonia 2017SGR278 (DS) and the Fundació La Marató de TV3 201627-30 (DS), all from Spain. The CBMSO receives institutional support from Fundación "Ramón Areces". The Prevención con Dieta Mediterránea (PREDIMED) trial was supported by grants from the agency for biomedical research of the Spanish government, the Instituto de Salud Carlos III RTIC G03/140, the Centro de Investigación Biomédica en Red de Fisiopatología de la Obesidad y Nutrición, the Centro Nacional de Investigaciones Cardiovasculares CNIC 06/2007, the Fondo de Investigación Sanitaria Fondo Europeo de Desarrollo Regional PI04-2239, PI 05/2584, CP06/00100, PI07/0240, PI07/1138, PI07/0954, PI 07/0473, PI10/01407, PI10/02658, PI11/01647, P11/02505, and PI13/00462, the Ministerio de Ciencia e Innovación AGL-2009–13906-C02 and AGL2010–22319-C03, the Fundación Mapfre 2010,

Consejería de Salud de la Junta de Andalucía PI0105/2007, the Public Health Division of the Department of Health of the Autonomous Government of Catalonia, Generalitat Valenciana ACOMP06109, GVA-COMP2010–181, GVACOMP2011–151, CS2010-AP-111, and CS2011-AP-042 and the Regional Government of Navarra P27/2011. Metabolomics measurements in PREDIMED were funded by the National Institutes of Health R01DK102896, F31DK114938, NIH/NHLBI 1R01HL118264, NIH/NHLBI 2R01HL118264. PREDIMED funding is related to MRC, FH, MA-MG and JS. VM was supported by pre-doctoral fellowships of the FPI Program (BES-2013-065986 and BES-2014-068929) from MINECO. We are grateful to the laboratories of Jorgina Satrustegui and José Manuel Cuezva for sharing the Seahorse equipment and Laura Santos for her help with histology procedures, from the laboratory of Marta Ruiz-Ortega at the Fundación Jiménez Díaz. We also thank the help of the following facilities of the CBMSO: animal housing, flow cytometry and confocal microscopy.

Competing interests

The authors have no conflicts of interest.

References

1 Kazancioglu, R. Risk factors for chronic kidney disease: an update. *Kidney Int Suppl (2011)* **3**, 368-371, doi:10.1038/kisup.2013.79 (2013).

2 Drawz, P. E. & Rosenberg, M. E. Slowing progression of chronic kidney disease. *Kidney Int Suppl (2011)* **3**, 372-376, doi:10.1038/kisup.2013.80 (2013).

3 Kang, H. M. *et al.* Defective fatty acid oxidation in renal tubular epithelial cells has a key role in kidney fibrosis development. *Nat Med* **21**, 37-46, doi:10.1038/nm.3762 (2015).

4 Chung, K. W. *et al.* Mitochondrial Damage and Activation of the STING Pathway Lead to Renal Inflammation and Fibrosis. *Cell Metab* **30**, 784-799 e785, doi:10.1016/j.cmet.2019.08.003 (2019).

5 Stadler, K., Goldberg, I. J. & Susztak, K. The evolving understanding of the contribution of lipid metabolism to diabetic kidney disease. *Curr Diab Rep* **15**, 40, doi:10.1007/s11892-015-0611-8 (2015).

6 Eirin, A., Lerman, A. & Lerman, L. O. The Emerging Role of Mitochondrial Targeting in Kidney Disease. *Handb Exp Pharmacol* **240**, 229-250, doi:10.1007/164_2016_6 (2017).

7 Mihaylova, M. M. & Shaw, R. J. The AMPK signalling pathway coordinates cell growth, autophagy and metabolism. *Nat Cell Biol* **13**, 1016-1023, doi:10.1038/ncb2329 (2011).

8 Imig, J. D. & Ryan, M. J. Immune and inflammatory role in renal disease. *Compr Physiol* **3**, 957-976, doi:10.1002/cphy.c120028 (2013).

9 Kusaba, T., Lalli, M., Kramann, R., Kobayashi, A. & Humphreys, B. D. Differentiated kidney epithelial cells repair injured proximal tubule. *Proc Natl Acad Sci U S A* **111**, 1527-1532, doi:10.1073/pnas.1310653110 (2014).

10 Grgic, I., Duffield, J. S. & Humphreys, B. D. The origin of interstitial myofibroblasts in chronic kidney disease. *Pediatr Nephrol* **27**, 183-193, doi:10.1007/s00467-011-1772-6 (2012).

11 Huang, S. & Susztak, K. Epithelial Plasticity versus EMT in Kidney Fibrosis. *Trends Mol Med* **22**, 4-6, doi:10.1016/j.molmed.2015.11.009 (2016).

12 Estruch, R. *et al.* Primary Prevention of Cardiovascular Disease with a Mediterranean Diet Supplemented with Extra-Virgin Olive Oil or Nuts. *N Engl J Med* **378**, e34, doi:10.1056/NEJMoa1800389 (2018).

13 Duann, P. & Lin, P. H. Mitochondria Damage and Kidney Disease. *Adv Exp Med Biol* **982**, 529-551, doi:10.1007/978-3-319-55330-6_27 (2017).

14 Afshinnia, F. *et al.* Impaired beta-Oxidation and Altered Complex Lipid Fatty Acid Partitioning with Advancing CKD. *J Am Soc Nephrol* **29**, 295-306, doi:10.1681/ASN.2017030350 (2018).

15 Hue, L. & Taegtmeyer, H. The Randle cycle revisited: a new head for an old hat. *Am J Physiol Endocrinol Metab* **297**, E578-591, doi:10.1152/ajpendo.00093.2009 (2009).

16 Mather, A. & Pollock, C. Glucose handling by the kidney. *Kidney Int Suppl*, S1-6, doi:10.1038/ki.2010.509 (2011).

17 Hochedlinger, K., Yamada, Y., Beard, C. & Jaenisch, R. Ectopic expression of Oct-4 blocks progenitor-cell differentiation and causes dysplasia in epithelial tissues. *Cell* **121**, 465-477, doi:10.1016/j.cell.2005.02.018 (2005).

18 Beard, C., Hochedlinger, K., Plath, K., Wutz, A. & Jaenisch, R. Efficient method to generate single-copy transgenic mice by site-specific integration in embryonic stem cells. *Genesis* **44**, 23-28, doi:10.1002/gene.20180 (2006).

19 Ly, J. P., Onay, T. & Quaggin, S. E. Mouse models to study kidney development, function and disease. *Current opinion in nephrology and hypertension* **20**, 382-390, doi:10.1097/MNH.0b013e328347cd4a (2011).

20 Kuzmichev, A. N. *et al.* Sox2 acts through Sox21 to regulate transcription in pluripotent and differentiated cells. *Curr Biol* **22**, 1705-1710, doi:10.1016/j.cub.2012.07.013 (2012).

21 Buchholz, F., Angrand, P. O. & Stewart, A. F. Improved properties of FLP recombinase evolved by cycling mutagenesis. *Nat Biotechnol* **16**, 657-662, doi:10.1038/nbt0798-657 (1998).

22 Kumar, R. M. *et al.* Deconstructing transcriptional heterogeneity in pluripotent stem cells. *Nature* **516**, 56-61, doi:10.1038/nature13920 (2014).

23 Livak, K. J. & Schmittgen, T. D. Analysis of relative gene expression data using real-time quantitative PCR and the 2(-Delta Delta C(T)) Method. *Methods* **25**, 402-408, doi:10.1006/meth.2001.1262 (2001).

24 Chevalier, R. L., Forbes, M. S. & Thornhill, B. A. Ureteral obstruction as a model of renal interstitial fibrosis and obstructive nephropathy. *Kidney Int* **75**, 1145-1152, doi:10.1038/ki.2009.86 (2009).

25 Fink, M., Henry, M. & Tange, J. D. Experimental folic acid nephropathy. *Pathology* **19**, 143-149 (1987).

26 Rahman, A. *et al.* A novel approach to adenine-induced chronic kidney disease associated anemia in rodents. *PLoS One* **13**, e0192531, doi:10.1371/journal.pone.0192531 (2018).

27 Huynh, F. K., Green, M. F., Koves, T. R. & Hirschey, M. D. Measurement of fatty acid oxidation rates in animal tissues and cell lines. *Methods Enzymol* **542**, 391-405, doi:10.1016/B978-0-12-416618-9.00020-0 (2014).

28 Misharin, A. V., Morales-Nebreda, L., Mutlu, G. M., Budinger, G. R. & Perlman, H. Flow cytometric analysis of macrophages and dendritic cell subsets in the mouse lung. *Am J Respir Cell Mol Biol* **49**, 503-510, doi:10.1165/rcmb.2013-0086MA (2013).

29 Smeets, B. *et al.* Proximal tubular cells contain a phenotypically distinct, scattered cell population involved in tubular regeneration. *J Pathol* **229**, 645-659, doi:10.1002/path.4125 (2013).

30 van der Windt, G. J., Chang, C. H. & Pearce, E. L. Measuring Bioenergetics in T Cells Using a Seahorse Extracellular Flux Analyzer. *Curr Protoc Immunol* **113**, 3 16B 11-13 16B 14, doi:10.1002/0471142735.im0316bs113 (2016).

31 Ravi, S. *et al.* Defining the effects of storage on platelet bioenergetics: The role of increased proton leak. *Biochim Biophys Acta* **1852**, 2525-2534, doi:10.1016/j.bbadis.2015.08.026 (2015).

32 Acebo, P. *et al.* Cancer abolishes the tissue type-specific differences in the phenotype of energetic metabolism. *Transl Oncol* **2**, 138-145 (2009).

33 Varga, J., Brenner, D. & Phan, S. (ed New Jersey: Humana Press) (2005).

34 Zoja, C. *et al.* How to fully protect the kidney in a severe model of progressive nephropathy: a multidrug approach. *J Am Soc Nephrol* **13**, 2898-2908 (2002).

35 Calderon-Dominguez, M. *et al.* Carnitine Palmitoyltransferase 1 Increases Lipolysis, UCP1 Protein Expression and Mitochondrial Activity in Brown Adipocytes. *PLoS One* **11**, e0159399, doi:10.1371/journal.pone.0159399 (2016).

36 Diaz-Lopez, A. *et al.* Cross-sectional associations between macronutrient intake and chronic kidney disease in a population at high cardiovascular risk. *Clin Nutr* **32**, 606-612, doi:10.1016/j.clnu.2012.10.013 (2013).

37 Beckerman, P. *et al.* Human Kidney Tubule-Specific Gene Expression Based Dissection of Chronic Kidney Disease Traits. *EBioMedicine* **24**, 267-276, doi:10.1016/j.ebiom.2017.09.014 (2017).

Figure Legends

Figure 1. Characterization of Dox-inducible Cpt1a gene overexpression in the transgenic mouse model for inducible *Cpt1a* gene in renal epithelial cells. (A) Schematic depicting the strategy to generate mice with inducible renal tubular epithelial-specific overexpression of CPT1A. Pax8-rtTA mice, which express the rtTA transactivator specifically in renal tubular epithelial cells driven by the Pax-8 promoter, were crossed with mice harboring the tetO-Cpt1a gene construction where the *Cpt1a* gene is under the control of a doxycycline-responsive promoter element. The yellow star indicates doxycycline-dependent activation of the transactivator. The construct bears an autoproteolytic P2A site, facilitating independent expressions of CPT1A and GFP (see text for details). **(B)** PCR analysis of offspring genotypes from these crosses. Genomic DNA analysis by PCR for the Pax8-rtTA allele generates a 595-pb band (¡Error! No se encuentra el origen de la referencia.). The GFP, Exon and FRT PCRs are described in Supplemental Figure 1a. Double heterozygous *Pax8-rtTA*$^{tg/0}$*:tetO-Cpt1a*$^{tg/0}$ mice (lane 1) were selected for experiments. **(C)** mRNA levels of *Cpt1a* gene was determined by qRT-PCR in total kidney tissue of mice treated with doxycycline for 3 weeks. Data represent the mean ± s.e.m (n = 6 mice per group). **P < 0.05 compared to kidneys from WT mice. **(D)** Immunoblots depicting protein levels of CPT1A and GFP in kidneys and livers of 3 individual mice per group. β-actin was used for normalization purposes. **(E)** Bar graphs represent the mean ± s.e.m of fold changes corresponding to densitometric analyses (n = 6 mice per group). **P < 0.01 compared to kidneys from WT mice. **(F)** Representative images of double immunofluorescence staining with the proximal tubular marker lotus tetragonolobus lectin (LTL), GFP, DAPI (nuclei) and merge of all three. **(G)** Staining with DAPI (nuclei), CPT1A and the mitochondrial marker ATP synthase beta-subunit (βF1). All panels show immunofluorescence images of kidneys from WT and Pax8-CPT1A mice after doxycycline administration. Scale bar: 100 µm (F and G). **(H)** Radiolabeled palmitate-derived CO_2 and

acid-soluble products (ASP) were determined after incubation of ^{14}C-palmitate with kidney tissue from WT or Pax8-CPT1A mice after doxycycline treatment. Bar graphs represent the mean ± s.e.m (n = 4 mice per group). *P < 0.05 compared to kidneys from WT mice. Statistical significance between two independent groups was determined using non-parametric two-tailed Mann-Whitney test, while more than two groups were compared with Kruskal-Wallis test.

Figure 2. CPT1A overexpression prevents FAN-associated kidney function deterioration and experimental renal fibrosis. (A) Representative microphotographs from one mouse per group of hematoxylin and eosin (H&E) (upper panels) and Sirius Red (lower panels) staining of kidneys from WT and Pax8-CPT1A mice subjected to FAN after doxycycline treatment (Dox). The fibrotic area is represented as Sirius Red staining of FA-treated mouse kidneys (FAN) related to control kidneys (C). Scale bars: 50 μm. Quantification of Sirius Red staining was calculated as a ratio of the stained area over the total area and bar graphs represent the mean ± s.e.m, n = 6 mice per group. *P < 0.05, compared to FAN/C kidneys in WT mice, respectively. **(B, C)** Serum blood urea nitrogen (BUN) **(B)** and serum creatinine **(C)** levels of WT and Pax8-CPT1A mice subjected to FAN after doxycycline treatment. Data represent the mean ± s.e.m (n = 6 mice per group). *P < 0.05, **P < 0.01 compared to its respective experimental control (CT) condition; $^{\#}$P < 0.05, compared to WT mice with the same experimental condition. **(D)** Immunoblots depicting fibronectin (FN), carnitine palmitoyltransferase 1A (CPT1A), green fluorescence protein (GFP) and alpha-smooth muscle actin (α-SMA) protein levels in kidneys from control (CT) and FA-treated (FAN) WT and Pax8-CPT1A mice after doxycycline induction. **(E)** Bar graphs represent the mean ± s.e.m. of fold changes corresponding to densitometric analyses (n = 6 mice per group). Glyceraldehyde-3-phosphate dehydrogenase (GAPDH) was used for normalization purposes. *P < 0.05, **P < 0.01 compared to their corresponding control (CT)

kidneys; $^{\#}P < 0.05$, $^{\#\#}P < 0.01$ compared to kidneys from WT mice with the same experimental condition. **(F)** mRNA levels of fibrosis-associated genes were determined by qRT-PCR using TaqMan qPCR probes in kidneys from control (CT) and FA-treated (FAN) WT and Pax8-CPT1A mice after doxycycline induction. Bar graphs represent the mean ± s.e.m. of fold changes (n = 6 mice per group). *P < 0.05, **P < 0.01 compared to their corresponding control (CT) kidneys; $^{\#\#}P < 0.01$ compared to kidneys from WT mice with the same experimental condition. Statistical significance between two independent groups was determined using non-parametric two-tailed Mann-Whitney test, while more than two groups were compared with Kruskal-Wallis test. For gene nomenclature see **Supplemental Table 4**.

Figure 3. CPT1A prevents impaired mitochondrial morphology and fatty acid oxidation defect in FAN-induced kidney fibrosis. (A) Representative electron microscopy images of cortical proximal tubules from control and Pax8-CPT1A mice subjected to FAN after doxycycline induction. Note reduced mitochondrial mass with a fragmented, small and round appearance in WT mice treated with FA. These changes were markedly abrogated in renal epithelial cells from mice overexpressing CPT1A. Scale bars: 10 µm (left panels), 500 nm (middle panels), 100 nm (right panels). Arrows point at representative mitochondria for each corresponding experimental condition. **(B)** Mitochondrial DNA copy number (mtDNA) was determined in kidneys of WT and Pax8-CPT1A mice in the UUO (3 and 7 days) and FAN models as specified in Methods. Bar graphs represent the mean ± s.e.m. of fold changes (n = 6 mice per group). **P < 0.01 compared to their corresponding control (CT) kidneys; $^{\#}P < 0.05$ compared to kidneys from WT mice with the same experimental condition. **(C)** Radiolabeled palmitate-derived CO_2 was determined after incubation of ^{14}C-palmitate with kidney tissue from WT and Pax8-CPT1A mice in the FAN model after doxycycline induction. **(D)** ATP levels in total kidney tissue determined in mice subjected to FAN model.

(C and D) Bar graphs represent the mean ± s.e.m (n = 4 mice per group). *P < 0.05, **P < 0.01 compared to their corresponding control (CT) kidneys; $^{\#}$P < 0.05 compared to kidneys from WT mice with the same experimental condition. **(E, F)** mRNA levels of glucose utilization-**(E)** and peroxisomal/mitochondrial function-**(F)** associated genes were determined by qRT-PCR using TaqMan qPCR probes in kidneys from control (CT) and FA-treated (FAN) WT and Pax8-CPT1A mice after doxycycline induction. (E and F) Bar graphs represent the mean ± s.e.m. of fold changes (n = 6 mice per group). *P < 0.05, **P < 0.01 compared to their corresponding control (CT) kidneys; $^{\#}$P < 0.05, $^{\#\#}$P < 0.01, compared to kidneys from WT mice with the same experimental condition. Statistical significance between two independent groups was determined using non-parametric two-tailed Kruskal-Wallis test. For detailed gene nomenclature see **Supplemental Table 4**.

Figure 4. CPT1A overexpression prevents TGF-β1-induced FAO impairment and epithelial cell dedifferentiation. (A) Bright field or GFP immunofluorescence images of primary kidney epithelial cells (TECs) isolated from kidneys of WT and Pax8-CPT1A mice. Scale bar, 20 µm. **(B)** Oxygen consumption rate (OCR) of TECs from WT mice was measured with a Seahorse XF24 Extracellular Flux Analyzer. Where indicated, cells were pre-treated with palmitate-BSA FAO Substrate (200 µM) or the CPT1 inhibitor Etomoxir (Eto, 400 µM). Oligomycin (1 µM), FCCP (3 µM) and a combination of antimycin A (1 µM) and rotenone (1 µM) (AA/Rot) were injected sequentially at the time points indicated. Data are represented after normalization by protein amount. Each data point represents the mean ± s.e.m of 4 independent experiments, each performed in triplicate. **(C)** Oxygen consumption rate (OCR) of TECs from WT and Pax8-CPT1A mice was measured with a Seahorse XF24 Extracellular Flux Analyser. Cells were pre-treated with palmitate-BSA FAO Substrate (200 mM). Where indicated, cells were treated with TGF-β (10 ng/ml). Oligomycin (1 µM), FCCP (3 µM) and a combination of antimycin A (1 µM) and rotenone (1 µM) (AA/Rot) were injected

sequentially at the time points indicated. Bar graphs (right panel) show the rates of OCR associated to basal, proton-leak, ATP-linked, maximum, reserve capacity and non-mitochondrial respiratory statuses. *P < 0.05 compared to their corresponding control (CT) TECs; #P < 0.05 compared to TECs from WT mice with the same experimental condition. **(D)** Extracellular acidification rate (ECAR) of cells treated as in (A). Data are normalized by protein amount. Each data point represents the mean ± s.e.m of 4 independent experiments, each performed in triplicate. Statistical significance between two independent groups was determined using non-parametric two-tailed Kruskal-Wallis test.

Figure 5. Overexpression of CPT1A reduces M1 macrophage infiltration in the FAN model. (A) Representative multiparameter flow cytometry dot plots showing the expression of CD45, a panleukocyte antigen also present in hematopoietic cells, monocytes and macrophages and F4/80, a surface marker expressed by monocytes and macrophages, in kidney cells from WT and Pax8-CPT1A mice subjected to FAN after doxycycline induction (upper panels) (one mouse per group is represented). CD86 and CD206 were used to determine the proportion of M1 and M2 macrophage subpopulations, respectively, in the total macrophage population (F4/80+, CD45+) (lower panels). **(B)** Numbers in quadrants indicate cell proportions in percent of cells that express both markers. Bar graph represents the percentage of kidney cells expressing CD86 (M1), CD206 (M2) or both (M1/M2) markers. Data represent mean ± s.e.m (n = 4 mice per group). #P < 0.05 compared to damaged kidneys from WT mice. **(C, D)** mRNA levels of inflammation-associated **(C)** and apoptosis-associated **(D)** genes were determined by qRT-PCR using TaqMan qPCR probes in kidneys from control (CT) and FA-treated (FAN) WT and Pax8-CPT1A mice after doxycycline induction. Bar graphs represent the mean ± s.e.m. of fold changes (n = 6 mice per group). (C and D) *P < 0.05, **P < 0.01compared to their corresponding control (CT) kidneys; #P < 0.05, ##P < 0.01 compared to kidneys from WT mice with the same experimental condition.

Statistical significance between two independent groups was determined using non-parametric two-tailed Mann-Whitney test, while more than two groups were compared with Kruskal-Wallis test. For detailed gene nomenclature see **Supplemental Table 4**.

Figure 6. CPT1A overexpression reduces epithelial cell damage in the FAN model. (A) Representative flow cytometry dot plots illustrating cell populations from obstructed kidneys of WT and Pax8-CPT1A mice subjected to FAN after doxycycline treatment. Cells were gated for CD45 negative (-)/Epithelial Cell Adhesion Molecule (EpCAM) positive (+) (upper panels) and then selected for the presence of CD24 (lower panels). **(B)** Numbers in quadrants indicate cell proportions in percent. SSC-A: Side Scatter Area. Data shown are representative of 4 mice per group. Bar graphs show the percentage of kidney cells positive for CD24. Data represent the mean ± s.e.m (n = 4 mice per group). *P < 0.05 compared to their corresponding control (CT) kidneys; $^{\#}$P < 0.05 compared to damaged kidneys in WT mice. Statistical significance between two independent groups was determined using non-parametric two-tailed Kruskal-Wallis test.

Figure 7. Plasma acylcarnitines and CPT1A levels in patients with CKD. (A-C) Correlation between baseline GFR values and plasma short-chain acylcarnitines **(A),** medium-chain acylcarnitines **(B)** and long-chain acylcarnitines **(C)** score in CKD patients with GFR<60. **(D-F)** Correlation between baseline GFR values and plasma short-chain acylcarnitines **(D),** medium-chain acylcarnitines **(E)** and long-chain acylcarnitines **(F)** score in CKD patients with GFR≥60. **(G)** Baseline acylcarnitine levels by CKD stage. **(H)** CPT1A levels in renal biopsies from control (con) and patients with chronic kidney disease (CKD), diabetic kidney disease (DKD), diabetes mellitus (DM) or hypertension (HTN). **(I,J)** Correlation between CPT1A kidney levels and eGFR **(I)** or fibrosis score **(J)**. (A - G) Chi-squared and Student´s t-test were used to compare categorical and quantitative variables,

respectively. (H) ANOVA test was used to assess the significance across different disease groups. Cor.test() function in R was used to get the Pearson's correlation and the corresponding P-values.

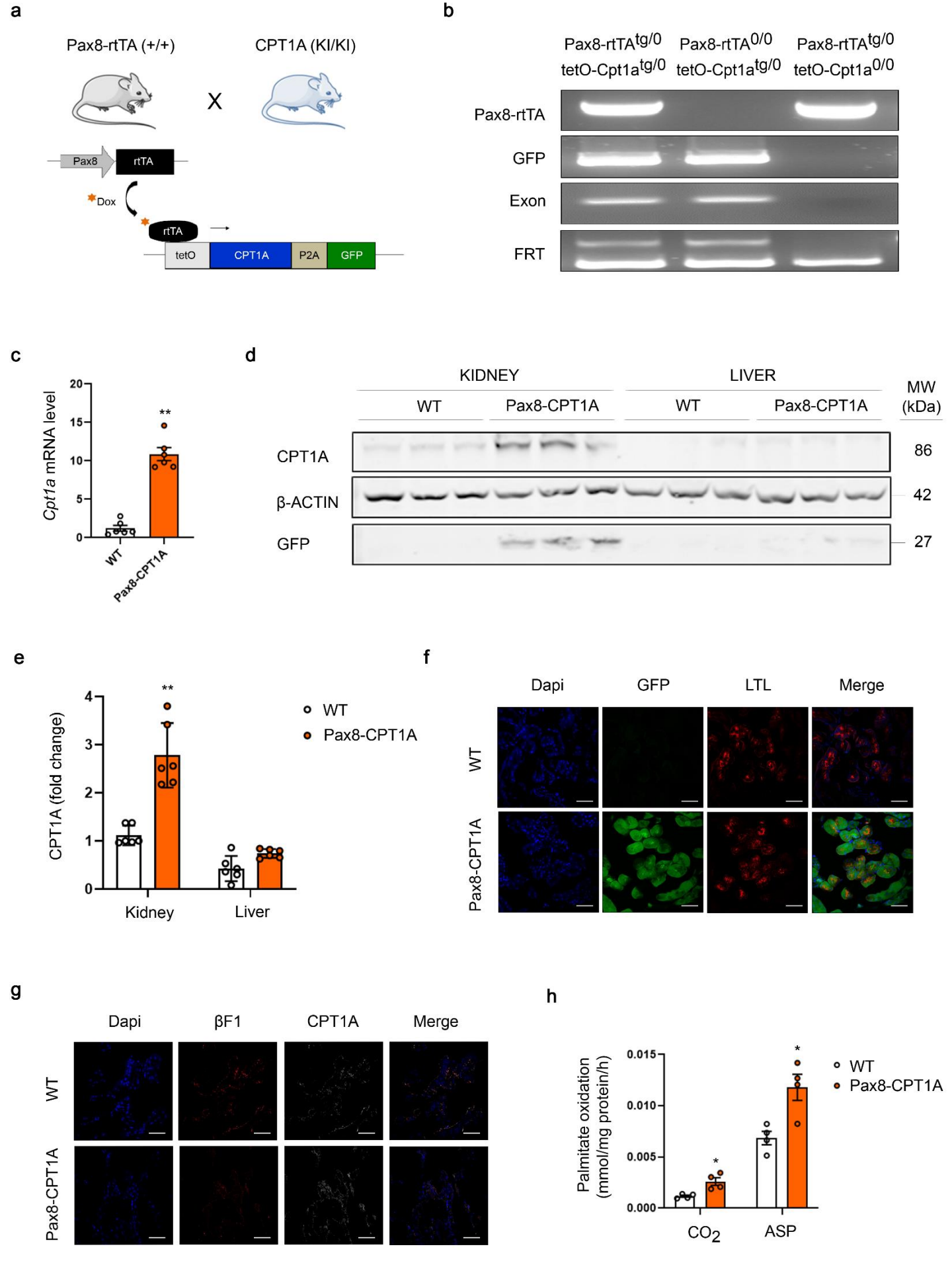

Figure 1

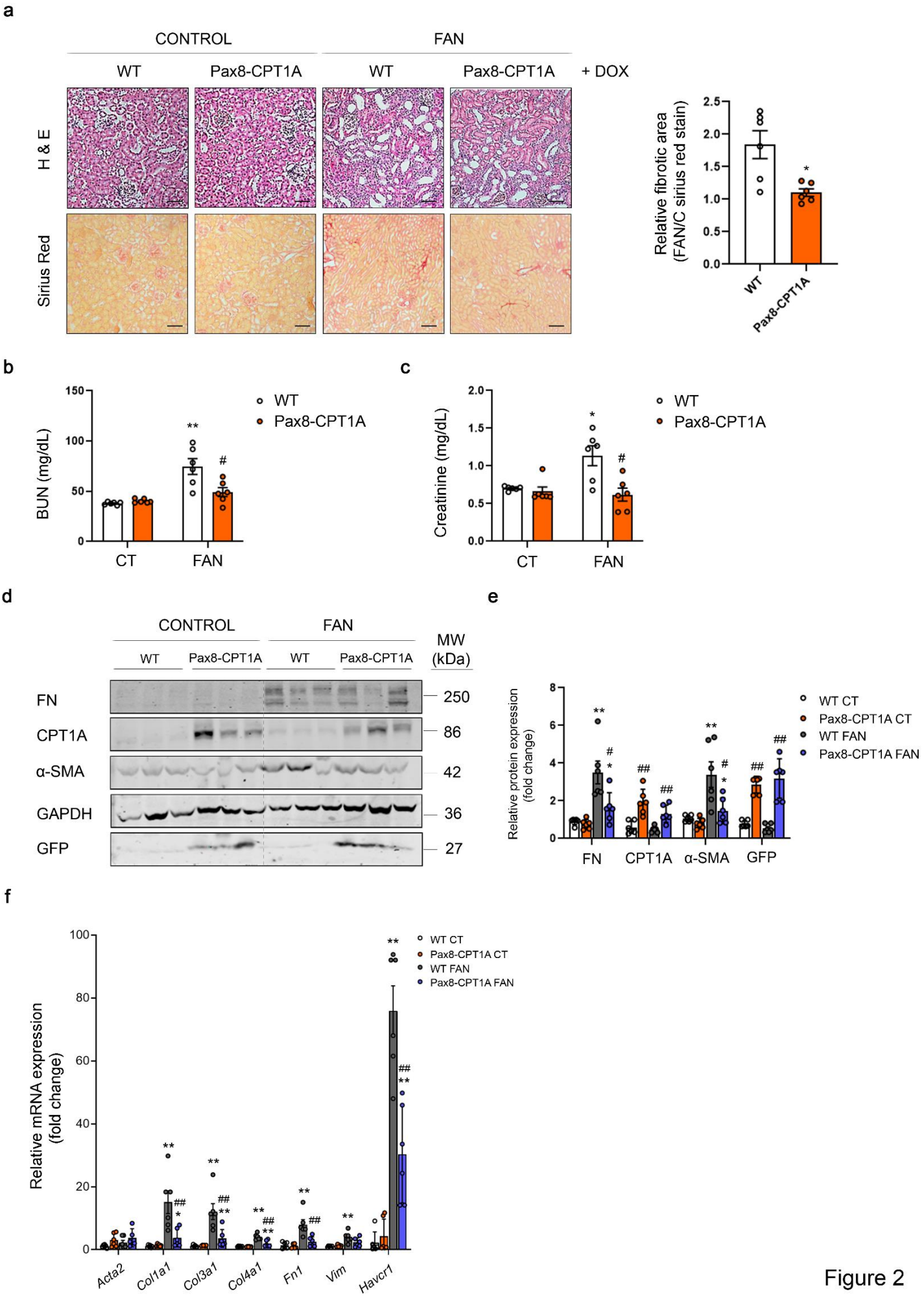

Figure 2

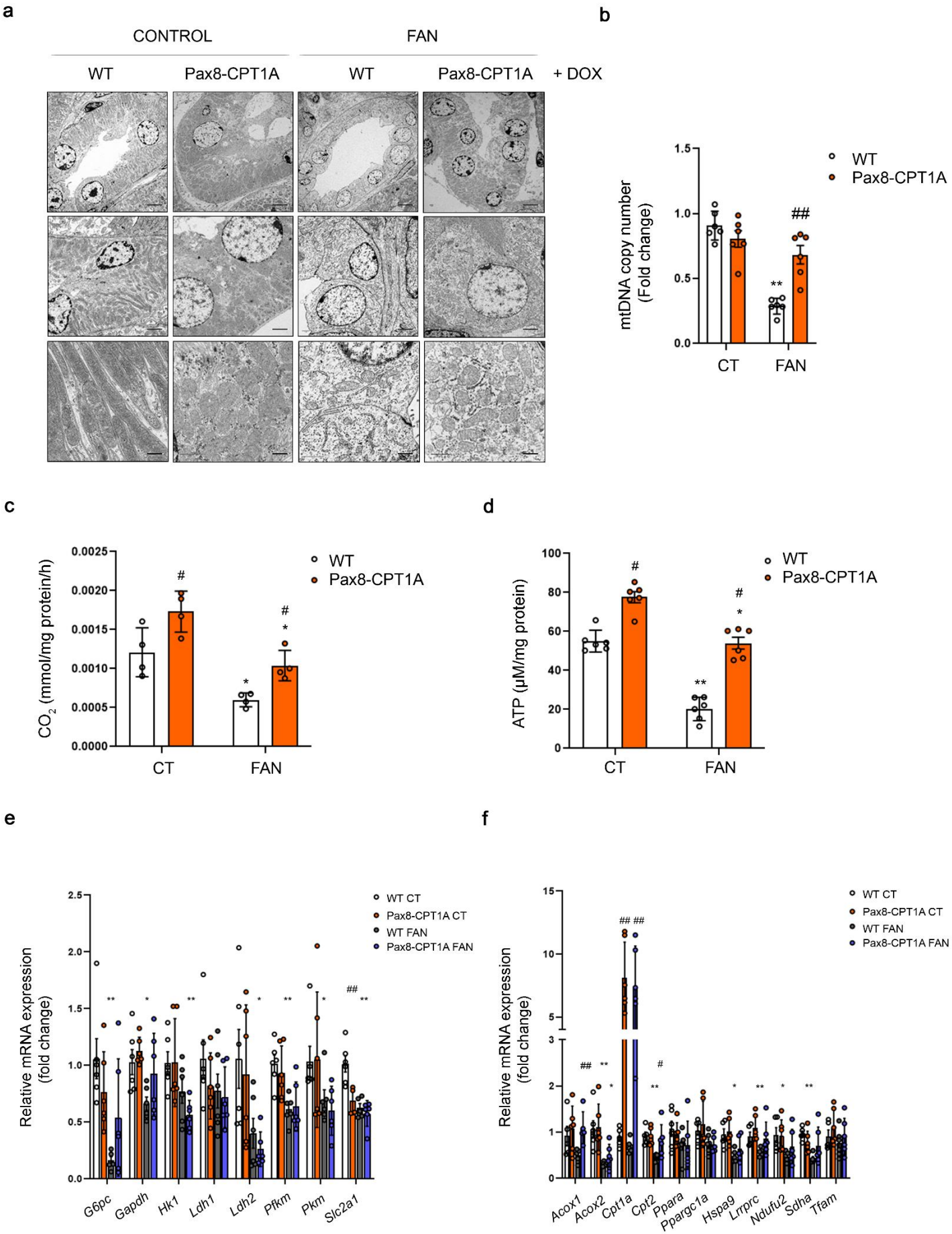

Figure 3

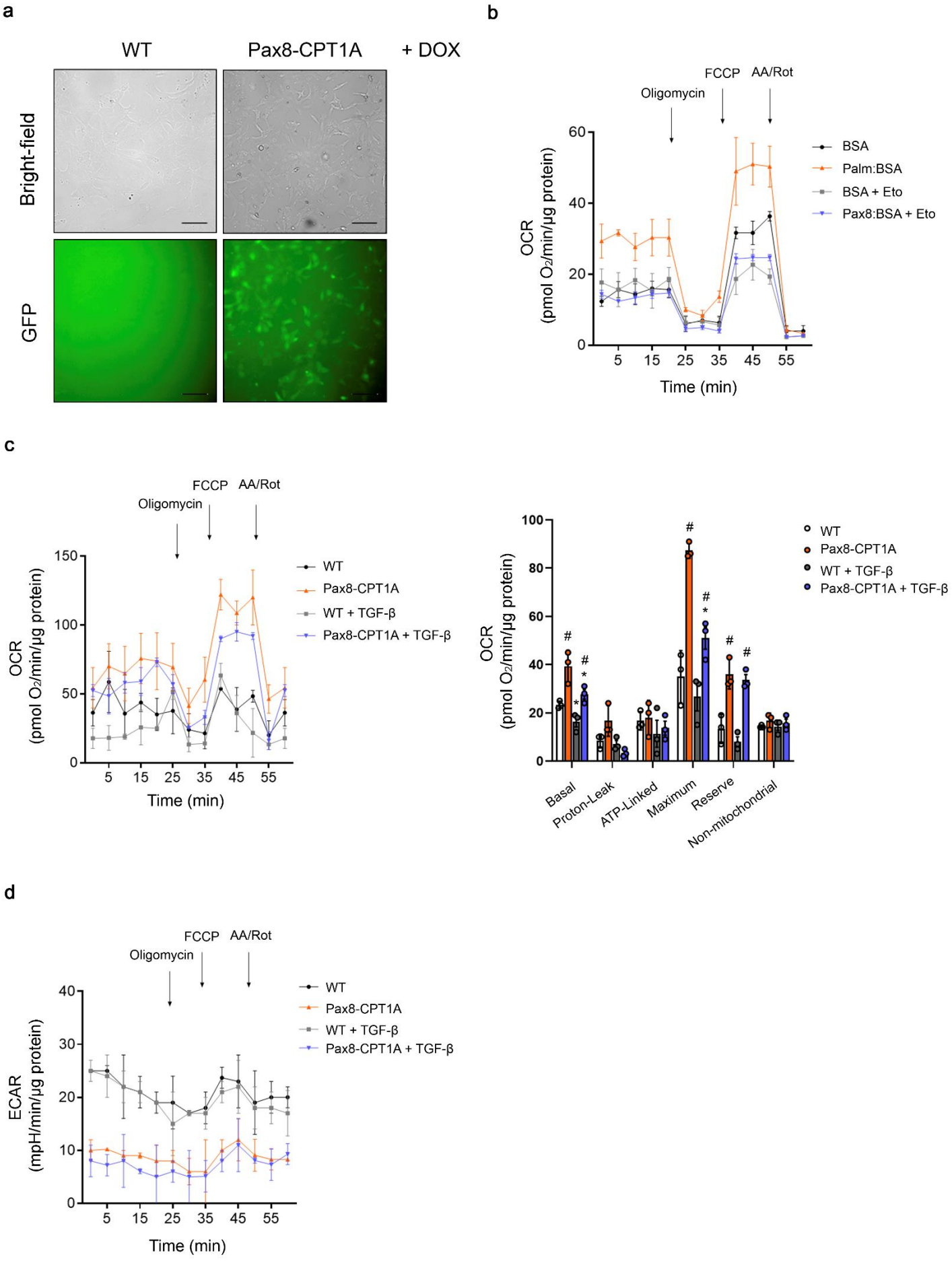

Figure 4

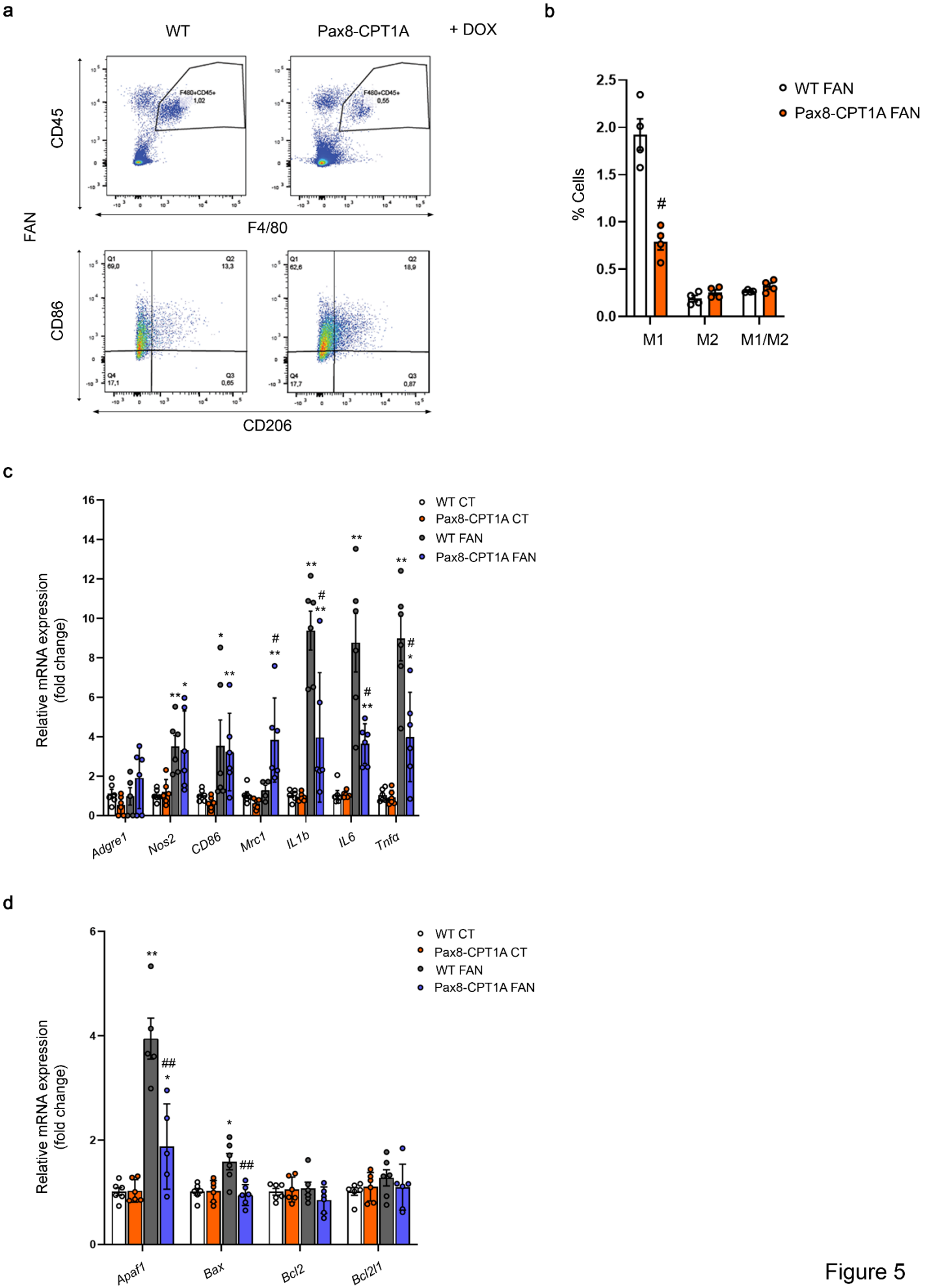

Figure 5

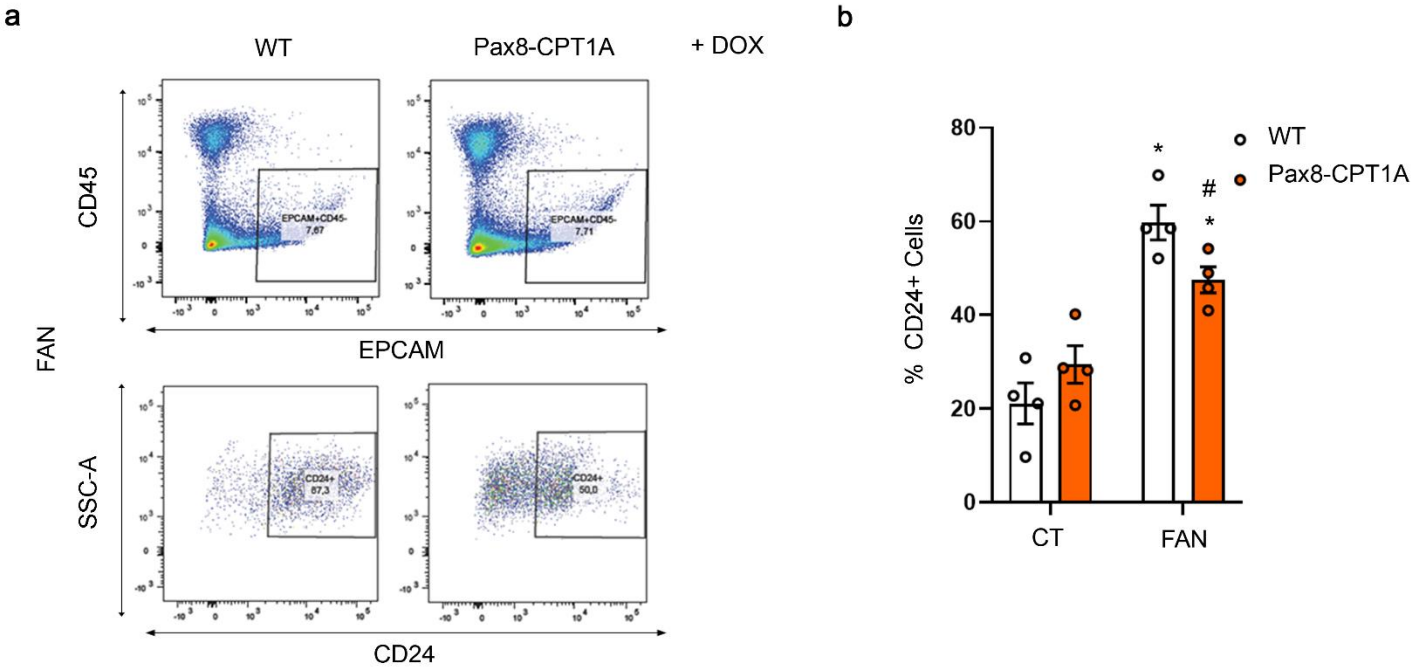

Figure 6

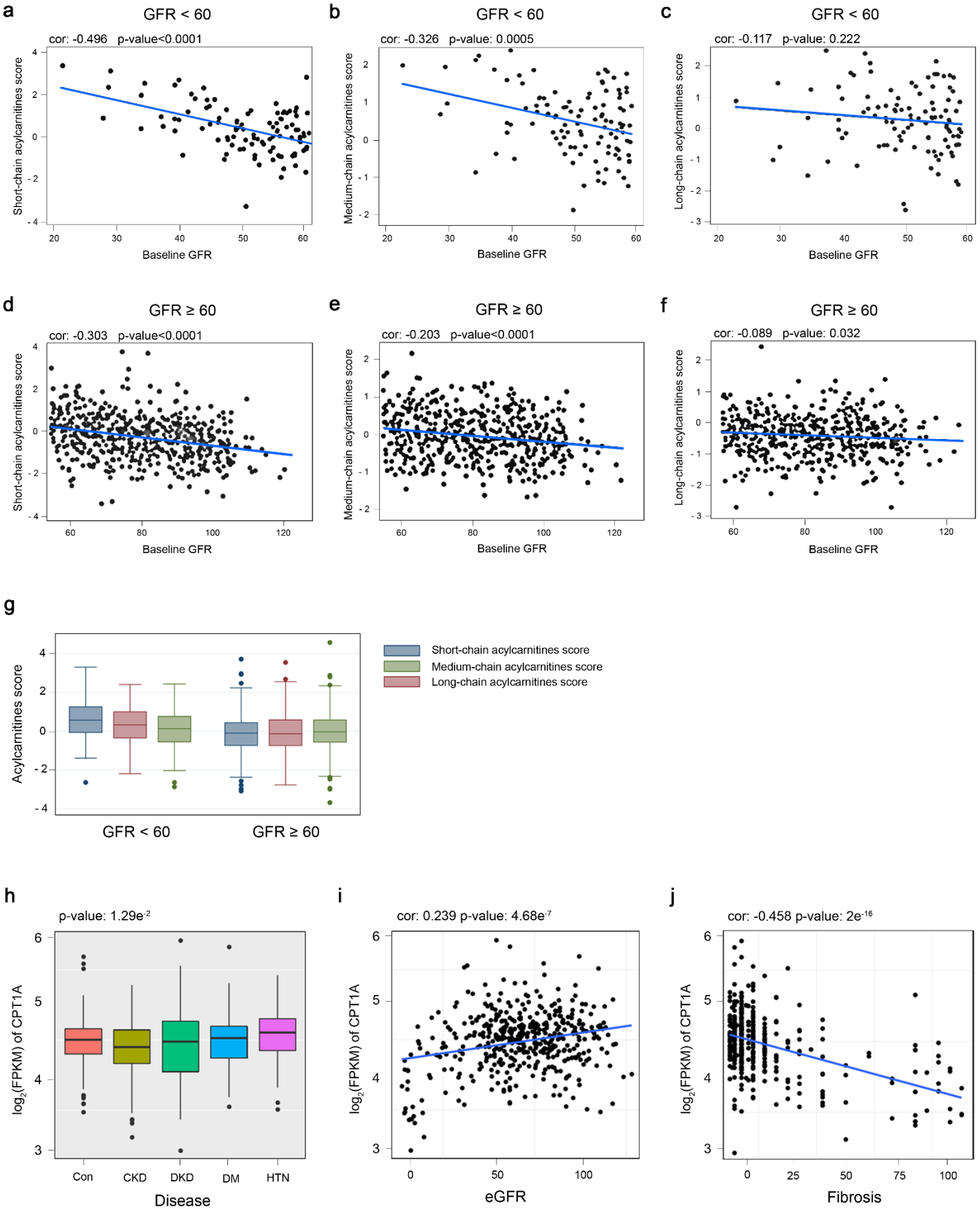

Figure 7